Recent and historical pollution legacy in high altitude Lake Marboré (Central Pyrenees): A record of mining and smelting since pre-Roman times in the Iberian Peninsula

J.P. Corella, M.J. Sierra, A. Garralón, R. Millan, J. Rodríguez-Alonso, M.P. Mata, A. Vicente de Vera, A. Moreno, P. González-Sampériz, B. Duval, et al.

Recent and historical pollution legacy in high altitude Lake Marboré (Central Pyrenees): a record of mining and smelting since pre-Roman times in the Iberian Peninsula

J.P. Corella[1*], M.J. Sierra[2], A. Garralón[2], R. Millán[2], J. Rodríguez-Alonso[2], M.P. Mata[3], A. Vicente de Vera[4], A. Moreno[4], P. González-Sampériz[4], B Duval[5], D. Amouroux[5], P. Vivez[6], C.A. Cuevas[7], J.A Adame[8], B. Wilhelm[1], A. Saiz-Lopez[7], B.L. Valero- Garcés[4]

[1]Universite Grenoble Alpes, CNRS, IRD, IGE, 38000 Grenoble, France.

[2]CIEMAT — Environmental Department (DMA), Avenida Complutense 40, E-28040 Madrid, Spain.

[3]Instituto Geológico y Minero de España, Rios Rosas 23, 28003 Madrid, Spain.

[4]Pyrenean Institute of Ecology, CSIC, Avda Montañana 1005, 50059 Zaragoza, Spain.

[5]Universite de Pau et des Pays de l'Adour, E2S UPPA, CNRS, IPREM, Institut des Sciences Analytiques et de Physico-chimie pour l'Environnement et les matériaux, Pau, France, 64000 Pau, France.

[6]Centro de Estudios de Sobrarbe, Sociedad Española para la Defensa del Patrimonio Geológico Y Minero, Plaza España, 22340 Boltaña, Huesca, Spain.

[7]Department of Atmospheric Chemistry and Climate, Institute of Physical Chemistry Rocasolano, CSIC, Serrano 119, 28006 Madrid, Spain.

[8]Atmospheric Sounding Station, El Arenosillo Observatory, Atmospheric Research and Instrumentation Branch, National Institute for Aerospace Technology (INTA), Mazagón, Huelva, Spain..

[*]Corresponding author: pcorella@iqfr.csic.es

ABSTRACT

We have analysed potential harmful trace elements (PHTE; Pb, Hg, Zn, As and Cu) on sediment cores retrieved from lake Marboré (LM) (2612 m a.s.l, 42°41'N; 0° 2'E). PHTE variability allowed us to reconstruct the timing and magnitude of trace metal

pollutants fluxes over the last 3000 years in the Central Pyrenees. A statistical treatment of the dataset (PCA) enabled us to discern the depositional processes of PHTE, that reach the lake via direct atmospheric deposition. Indeed, the location of LM above the atmospheric boundary layer makes this lake an exceptional site to record the long-range transport of atmospheric pollutants in the free troposphere. Air masses back-trajectories analyses enabled us to understand the transport pathways of atmospheric pollutants while lead isotopic analyses contributed to evaluate the source areas of metal pollution in SW Europe during the Late Holocene. PHTE variability, shows a clear agreement with the main exploitation phases of metal resources in Southern Europe during the Pre-Industrial Period. We observed an abrupt lead enrichment from 20 to 375 yrs CE mostly associated to silver and lead mining and smelting practices in Southern Iberia during the Roman Empire. This geochemical data suggests that regional atmospheric metal pollution during the Roman times rivalled the Industrial Period. PHTE also increased during the High and Late Middle Ages (10-15th centuries) associated to a reactivation of mining and metallurgy activities in high altitude Pyrenean mining sites during climate amelioration phases. Atmospheric mercury deposition in the Lake Marboré record mostly reflects global emissions, particularly from Almadén mines (central Spain) and slightly fluctuates during the last three millennia with a significant increase during the last five centuries. Our findings reveal a strong mining-related pollution legacy in alpine lakes and watersheds that needs to be considered in management plans for mountain ecosystems as global warming and human pressure effects may contribute to their future degradation.

KEY WORDS: Atmospheric pollution, lakes, trace metals, historical mining, Pyrenees

1- INTRODUCTION

Metallurgy has been key for the development of human society during Pre-industrial times (Killick and Fenn, 2012). The Iberian Peninsula is particularly rich in mineral resources and has a long history of mining and smelting activities with several of the world´s most representative historical mining districts. Almadén mines, located in Central Spain, has been the World´s largest mercury (Hg) mine until its closure at the turn of this century. This mine has been actively exploited during two millennia producing 30 % of the globally mined Hg with an accumulated historic Hg emission estimate of 10 000 tons (Hylander and Meili, 2003). Southern Iberia is also very rich in mineral resources hosting important silver (Ag) and lead (Pb) mining hotspots. These resources have been exploited for several millennia, with more than 10 000 tons of Pb produced contributing to 40 % of the World´s total lead production between 1200 BCE (before Common Era) and 500 CE (Common Era). Most of the Iberian Ag and Pb mining located in Rio Tinto and Mazarrón-Cartagena mining districts were intensively exploited by Phoenicians, Carthaginians and Romans.

In NW Iberia, mining and metallurgy started in the Chalcolithic–Early Bronze Age 4500 years ago according to archaeological information (de Blas, 1996, 2005) although the first atmospheric pollution signal related to these human activities has been dated 500 years before (~5 kyrs ago) (Martínez-Cortizas et al., 2016). To a lesser extent, the Pyrenees has also been largely exploited during the last centuries for Ag and Pb production (e.g. Arditurri mines in Western Pyrenees (Thalacker, 1804), Emporion mines in Catalonia (Montero-Ruiz et al., 2007)). Southern Central Pyrenees also have local rich deposits of metals including copper (Cu), Pb, Ag and iron (Fe), many of them historically mined and processed at high elevation emplacements (>2000 m a.s.l.) (e.g.

Bielsa-Parzán mining district (Calvo, 2008; Nieto-Callen, 1996)), although the timeline of their activities is not well constrain prior to the last 500 years.

Unfortunately, historical mining and metalworking activities have left a long-lasting imprint on the environment (Hansson et al., 2019). Indeed, although numerous natural and anthropogenic activities can increase contaminant levels in the environment, mining operations are notable regarding the number of particulates generated, the global impact, and the trace metals´ toxicity associated with atmospheric pollutant emissions (Csavina et al., 2012). Thus, large quantities of PHTE such as Pb, Hg, Cu, zinc (Zn) or arsenic (As) have been released to the regional atmosphere during the last millennia and subsequently deposited and stored in the Iberian Peninsula (Gallego et al., 2019; Hanebuth et al., 2018; Kylander et al., 2005; Leblanc et al., 2000; Manteca et al., 2017; Martínez-Cortizas et al., 1999; 2002; 2012; 2013; 2016; Mil-Homens et al., 2017; Serrano et al., 2013) among others, and elsewhere in the Northern Hemisphere even in remote, pristine glacier ice in the Alps and the Arctic (Hong et al., 1994, 1996; McConnell et al., 2018; 2019; Preunkert et al., 2019; Rosman et al., 1997), regions located far away from the pollution source. Understanding this environmental legacy, i.e. the persistence of PHTE pollution overtime from past anthropogenic emissions, and the fluxes from terrestrial to aquatic ecosystems (Bacardit and Camarero, 2010) should help environmental policy makers to design future and sustainable environmental management plans and monitoring programs. Indeed, as recently highlighted by Camarero (2017) and Le Roux et al. (2019), the long-term PHTE monitoring provided by natural archives is particularly needed in mountain environments such as the Pyrenees in order to assess the response of mountain critical zones to Global Change

Among natural archives, lake sediments have been widely used to reconstruct past mining and metalworking activities as well as other anthropogenic sources, e.g. (Cooke et al., 2011, 2020; Díez et al., 2017; Elbaz-Poulichet et al., 2020; Mariet et al., 2018; Renberg et al., 1994; Thevenon et al., 2011; Wilhelm et al., 2017). These continuous sedimentary records allow us to understand the variability of different mining-related pollution sources through time as well as to assess their environmental legacy. Surprisingly, yet relatively few pollution records from lacustrine sediments exist in the Iberian Peninsula (Camarero, 2017; Camarero et al., 1998; Corella et al., 2017; 2018; García-Alix et al., 2013; Hillman et al., 2017; Martín-Puertas et al., 2010). High-altitude mountain lakes record most efficiently past atmospheric pollution phases due to enhanced atmospheric precipitation and the "cold trapping" effect caused by elevation making these locations regional convergence areas of atmospheric pollutants (Camarero, 2017). Recent depositional patterns based on lake surface sediments show a W-E distribution with higher trace metal concentrations in the eastern Pyrenees lakes (Bacardit and Camarero, 2009; Camarero, 2003, 2017). Inventories of trace metals in soils and sediments in several lake catchments in the central Pyrenees have shown a large anthropogenic component (Bacardit and Camarero, 2010; Bacardit et al., 2012). High levels of pre-industrial pollutants have been reported in several Pyrenean lakes (Camarero et al., 1998; Lavilla et al., 2006), but millennial- long, well-dated records are scarce (Hansson et al., 2017). Recent research in several well-dated records from mountain lakes across an altitudinal transect in the Southern Central Pyrenees (NE Spain) assessed the variable pollutant loading in these ecosystems during the Industrial period (Corella et al., 2018). This study highlighted that among all studied lakes, high-altitude, pristine Lake Marboré (LM), located at the Pyrenean summit (> 2600 m. a.s.l.) records most efficiently past regional atmospheric deposition of PTHE. LM has

provided the sedimentary record at the highest altitude in the Pyrenees (Leunda et al., 2017; Oliva-Urcia et al., 2018) in a privileged location in the free troposphere. Therefore, LM record can be considered as representative of background, global atmospheric pollution since long-range transport of atmospheric pollutants mostly takes place above the atmospheric boundary layer.

This study aims to reconstruct the atmospheric pollution in the Pyrenees related to mining and metalworking activities in the Iberian Peninsula during the main historic periods of the last three millennia (namely Iron Age (IA; 1000 BCE- 218 BCE), Roman Period (RP; 218 BCE-476 CE), Early Middle Ages (EMA; 476-1000 CE), High Middle Ages (HMA; 1000-1300 CE), and Late Middle Ages (LMA; 1300-1492 CE), Modern Period and beginning of Contemporary Age (MP; 1492-1850 CE) and the Industrial Period (IP; 1850 CE-Present day). To achieve this goal, we have carried out a multi-proxy research strategy on the first 175 cm of a sediment core retrieved in the distal are of LM that comprises the last 3000 years. The multidisciplinary analyses included i) the determination of major, minor and trace metals that allowed us to quantify the geochemical composition of the sediments down-core; ii) lead isotopic analyses to evaluate the possible sources of metal pollution during the different historical phases of mining production in the Iberian Peninsula, iii) multivariate statistical modelling to discern the depositional processes of each geochemical element and iv) air masses back-trajectories computation to evaluate the atmospheric transport pathways of major pollutants during the last decades.

2-STUDY SITE

LM (42°41' N; 0° 2' E, Fig. 1) is a lake emplaced at 2612 m a.s.l. within a glacier cirque located in the Spanish Central Pyrenees. The lake has a surface area of 14.3 ha and it is

148 emplaced in a watershed of 137 ha (Valero-Garcés et al., 2013), lying on Cretaceous-
149 Tertiary carbonated rocks (Pujalte et al., 2016; Samsó Escolá and Robador, 2018). Mean
150 annual temperature and precipitation at the nearest meteorological station (Góriz station,
151 located at 2220 m a.s.l.) are 4.9ºC and ~2000 mm (Leunda et al., 2017). The vegetation
152 cover around the lake is very scarce with only a few patches of alpine herbs (Leunda et
153 al., 2017). The lake has a maximum depth of 30 m and an elongated morphology with
154 ~500 m along the WNW-ESE axis and ~200 m across (Sánchez-España et al., 2018).
155 Since there is no direct connection with the nearby Monte Perdido and Marboré glaciers
156 (García-Ruiz et al., 2014), lake level is controlled mostly by precipitation/evaporation
157 balance (Nicolás-Martínez, 2013; Valero-Garcés et al., 2013) with small ephemeral
158 inlets and outlets located in the lake´s western and southern shores respectively. The
159 lake was dammed in the 1940s but the dam was never completely functional and it has
160 been decommissioned. LM is a cold dimictic and ultra-oligotrophic lake which surface
161 is covered by ice and snow from December to July (Sánchez-España et al., 2018).
162

163 # 3- MATERIAL AND METHODS

164 **3.1- Back-trajectories analyses**. To estimate the atmospheric transport pathways to
165 LM, the back trajectories of air masses were computed using the HYSPLIT (Hybrid
166 Single-Particle Lagrangian Integrated Trajectory) model developed by NOAA's Air
167 Resources Laboratory (ARL) (Draxler et al., 2009). The HYSPLIT model is a complete
168 software for computing simple air parcel trajectories as well as complex transport,
169 dispersion, chemical transformation, and deposition simulations (Draxler et al., 2009). It
170 is often used for forward and back-trajectory air masses analysis, and to establish
171 source–receptor relationships (Stein et al., 2015). The calculation method is a hybrid

method between the Lagrangian approach, using a moving frame of reference for advection and diffusion calculations as the trajectories on air parcels move from their origin, and the Eulerian methodology using a fixed three-dimensional grid as a frame of reference to compute pollutant air concentrations (Stein et al., 2015). Three-dimensional kinematic trajectories were computed daily at 12:00 UTC, with a 72-hour runtime at 100 m above ground level (agl), taking as arrival point the LM. The back trajectories were calculated using the meteorological fields of the global meteorological model ECMWF (European Centre for Medium Range Weather Forecasts). In order to cover the entire studied period, we used ERA40 and ERA-Interim data reanalysis with similar spatial and temporal resolutions. The data reanalysis used has a spatial resolution of 0.5º (latitude x longitude), 22 vertical levels from the surface to 250 mb and a temporal resolution of 6 h. The back trajectories were calculated every six hours during the period 1960-2016 CE. Although climate variability has caused changes in weather conditions and extreme events at local and regional scale and also affected the intensity of atmospheric circulation dynamics during the Late Holocene (Sánchez-López et al., 2016), we assumed that general atmospheric circulation patterns has remained similar, and therefore, that 20-21st century air masses back trajectories are representative of the studied period (i.e. last 3000 years). ERA40 data reanalysis were used for the computation of back trajectories for the period 1960- 1993 CE, while ERA-Interim for the period 1994-2016 yrs CE (Dee et al., 2011). These meteorological fields were converted into the ARL standard format using the HYSPLIT model. Back-trajectories from 1960 to 2016 yrs CE have been added on a 0.25º×0.25º grid to visualize air masses sources (frequency map shown in Fig 1). Frequency map represents the number of back-trajectories passing above every location before arriving to LM in the 1960-2016 yrs CE time period. To estimate the main source areas of these

197 trajectories arriving to LM we have defined several regions and calculated the number
198 of trajectories passing through those regions before arriving to LM (Table 1). Note that
199 since back-trajectories pass above more than one region before arriving to LM, the sum
200 of all percentages does not equal 100%. For calculation of specific emission sources
201 (i.e. mining districts) we have considered for each site an area equal to its location ± 2º
202 (latitude and longitude).
203
204 **3.2- Sediment cores and age-depth model.** A long (~7 m) sediment core (MAR11-
205 1U) and a short (0,2 m) gravity (MAR11-1G-1U) were retrieved in august 2011 from
206 the deepest part of LM using an UWITEC floating platform and coring equipment from
207 the Pyrenean Institute of Ecology (IPE-CSIC) (Oliva-Urcia et al., 2018). Core
208 correlation between the short and the long core was carried out using the Pb
209 concentration profiles (Oliva-Urcia et al., 2018). For the development of the composite
210 UWITEC sedimentary sequence we used consecutive sections since the recovery factor
211 was excellent. Sediment cores were split lengthwise for sedimentary facies description
212 and discrete sampling. A continuous sampling was carried out every 2 cm was carried
213 out for geochemical analyses. LM sediments during the Late Holocene mainly consists
214 of laminated siliciclastic mud with very low Total Organic Carbon content (TOC
215 ranging from 0.1 to 1.1%) (Corella et al., 2018; Oliva-Urcia et al., 2018; Valero-Garcés
216 et al., 2013). Recent sedimentation has been characterized with sediment traps located
217 in the deeper areas of the lake since 2017. Annual surveys include water sampling and
218 temperature, pH, conductivity and oxygen depth profiles.
219 The chronology for the Late Holocene sediment sequence in LM was developed
220 using five Accelerator Mass Spectrometry (AMS) ^{14}C radiometric dates from long core
221 MAR11-1U and $^{137}Cs/^{210}Pb$ dating performed from the gravity core MAR11-1G-1U.

222 ^{210}Pb dating in the short core was obtained by gamma ray spectrometry. Excess
223 (unsupported) ^{210}Pb was calculated by the difference between total ^{210}Pb and ^{214}Pb for
224 individual core intervals. ^{210}Pb chronology was determined using the constant rate of
225 supply (CRS) model (Appleby, 2001). The ^{210}Pb age model is supported by the presence
226 of a ^{137}Cs peak at 6 cm (AD 1963) in agreement with the ^{210}Pb chronology (Leunda et
227 al., 2017; Oliva-Urcia et al., 2018). The age-depth model has been constructed by linear
228 interpolation between the median ages of the probability distribution of adjacent
229 calibrated dates (see Leunda et al., (2017) and Oliva-Urcia et al., (2018)) for a complete
230 description and information of the LM age-depth model). In this study we have focused
231 in the upper 175 cm of the studied sedimentary sequence that comprises the period 1032
232 yrs BCE - 2010 yrs (CE) with mean sedimentation rates of 0.06 mm yr^{-1}.
233
234 **3.3- Geochemical and geophysical analyses.** Al, As, B, Ba, Ca, Cd, Cr, Cu, Fe, K, Mg,
235 Mn, P, Pb, Si, Sr, Ti, Zn, and Zr concentration were analyzed in 91 samples by optical
236 emission spectrometry using inductively coupled plasma-atomic emission spectroscopy
237 (ICP-OES; Thermo ICP-OES iCAP 6300 DUO-Thermo Fisher Scientific, Waltham,
238 MA, USA) at the IPE-CSIC laboratories. Samples were previously digested with HNO_3
239 (9 ml) and HCl (3 ml) in a microwave oven 'BERGHOF MWS'. Total Hg concentration
240 measurements were carried out by Atomic Absorption Spectrophotometry using an
241 Advance Mercury Analyzer (AMA 254, LECO Company). This equipment is
242 specifically designed for the direct mercury determination in solid and liquid samples
243 without a need of sample chemical pre-treatment. Certified reference material (CRM)
244 were used to determine the accuracy and precision of the Hg measurements (NCS
245 DC87103, soil, [Hg] = 0.017 ± 0.003 mg kg^{-1}). The repeatability was Sr ≤ 15 % and the
246 relative uncertainty associated with the method (k = 2) was ± 20%. All analyses were

247 run at least in triplicate. Total Carbon (TC), Total Organic Carbon (TOC) and Total
248 Inorganic Carbon (TIC) had been previously determined with a LECO SC 144 DR
249 elemental analyzer (Oliva-Urcia et al., 2018). TIC values were obtained by subtracting
250 TOC from TC (Fig. 2).

251 Principal Component Analyses (PCA) were applied to reduce the large
252 geochemical dataset into a smaller number of variables (i.e. principal components (PC)
253 helping to interpret environmental and depositional processes. PCA was carried out
254 including all the elements (Cu, Zn, Cd, Mn, Ca, Fe, P, As, Hg, Pb, Sr, Zr, Si, Cr, Mg, Ti,
255 B, K, Al and Ba) using trace metals´ concentrations (Fig. 3) and accumulation rates
256 (Fig. S1). The PCA was performed with varimax rotation over the geochemical dataset
257 using the SPSS 23.0 software. To calculate Enrichment Factors (EFs), firstly, all the
258 PTHE have been normalized to aluminum (Al) in order to confirm that the changes in
259 metals concentrations are not related to detrital input variability. Al has been selected for
260 normalization since this lithogenic element is immobile (i.e. geochemically stable) in
261 the sediments and it is abundant in carbonated watersheds (Boës et al., 2011; Tylmann,
262 2005). Later, EFs have been calculated using the average element concentrations before
263 1000 BCE as baseline conditions which may differ from natural background values. EFs
264 have been estimated to identify and quantify anthropogenic interferences in natural
265 element cycles (Amos et al., 2015; Biester et al., 2007; Weiss et al., 1999).
266

267 $$EF = \frac{[M_{cm}]/[Al_{cm}]}{[M_{bottom}]/[Al_{bottom}]}$$

268

269 $[M_{cm}]$ and $[Al_{cm}]$ represent the metal and aluminum fluxes at the same depths of the
270 sediment cores while $[M_{bottom}]$ and $[Al_{bottom}]$ are the metal and aluminum fluxes in the

271 basal sediments of the sediment cores in LM. Hg EF has been calculated as the ratio
272 between the [Hg] in a given sample by the average [Hg] in the section below 1000 BCE
273 following Biester et al. (2007)
274
275 **3.4- Pb isotopic analyses.** Pb isotope ratios are commonly used as tracers of both
276 natural and anthropogenic sources of metals recorded in natural archives (Komárek et
277 al., 2008). In order to shed light on the origin of Pb pollution found in the LM record,
278 45 samples were collected for Pb isotopic analyses. A 0.1 g of powdered rock was
279 digested overnight in HNO_3 and evaporated to dryness. The residue is dissolved in 0.5
280 M ammonium acetate, and Pb separated of the major cations by conventional ion-
281 exchange chromatography (DigiSEP Blue, SCP Science). The recovered Pb is
282 evaporated to dryness, dissolved in 0.5 M HNO_3 and diluted to a final concentration of
283 100–200 ppb. The samples were measured using the standard bracketing method. ICP-
284 MS measurements were carried out with an Element 2 SF-ICP-MS (Thermo Finnigan,
285 Bremen, Germany) equipped with a guard electrode to eliminate secondary discharge in
286 the plasma and to enhance overall sensitivity. The high resolution double focusing
287 (reverse Niers–Johnson geometry) single collector ICP-MS instrument provides flat top
288 peaks in the low resolution mode (m/Δm 300) which was used for the analysis of ^{202} Hg,
289 ^{204}Pb, ^{206}Pb, ^{207}Pb and ^{208}Pb. A micro volume autosampler (SC-2 DX FAST
290 Autosampler, ESI Inc., Omaha, NE, USA) and a sample introduction kit consisting of a
291 PFA microflow nebulizer, a Peltier-cooled spray cyclonic chamber and a sapphire
292 injector tube (ESI Inc., Omaha, NE, USA) were employed to transport the samples into
293 the plasma of the ICP-MS. This configuration increases the sensitivity and stability of
294 the conventional sample introduction setup. Samples were diluted ten times with 2 %
295 (v/v) high purity HNO_3 to reduce the risk of clogging. The solutions were introduced

into the plasma using a PFA nebuliser, operating in self-aspiration mode at a flow rate of 50 mL/min. Regarding reagents and standards, all the solutions were prepared with high purity water (18.2 MV cm) from Milli-Q element system designed for ultra-trace analysis (Millipore, Milford, MA, USA). Nitric acid (65%, analytical-reagent grade, Scharlab, Barcelona, Spain) was further purified by sub-boiling distillation (DST-1000 Sub-Boiling Distillation System, Savillex Corporation, USA). Standard calibration solutions were prepared by appropriate dilution of a dissolved amount of NIST 981 certified standard (Inorganic Ventures) with 2% high-purity nitric acid.

4- RESULTS AND DISCUSSION

4.1. Concentrations and depositional processes of trace metals in LM.

4.1.1. Recent depositional processes: ice phenology, run-off and lake processes

Recent sediments in the deeper areas of LM characterized with sediment traps consist of siliciclastic silt, with about 1.1 % TOC, no carbonate and 0.05 % TS. Although carbonate-bearing formations occur in the watershed and the moraine deposits, the sediments in the lake are mostly devoid of carbonates (Oliva-Urcia et al., 2018). Mineral composition of the sediments is dominated by quartz, micas and detrital clay minerals, with presence of minor sulfides and other heavy minerals (mainly titanium oxides and zircon), all more resistant to weathering processes. Based on sediment traps data, the calculated sediment fluxes range between 390 g m^2 yr^{-1} in the more proximal zones closer to the NW inlet to 250 g m^2 yr^{-1} in the more distal areas. Microscope smear slide observations of recent sediments show the sporadic presence of heavy minerals in

the sediments (pyrite, galena, sphalerite and barite) indicative of occasional contributions from the watershed. High- Fe and Zn values have been found in the water column analysis in the thermocline in the ice-free period, being interpreted as a result of weathering reactions involving sulfides in the watershed (Sánchez-España et al., 2018). However, the influx of heavy metals into the lake due to run-off processes is expected to be small and likely constant during the last millennia as the composition of the surface sediment in LM drainage are remained the same in spite of glacier advances and retreats outside the watershed retreat (García-Ruiz et al., 2015).

The Iberian Peninsula has experienced different climatic periods during the Late Holocene (namely the Ibero-Roman Humid Period (IRHP), Dark Ages Cold Period (DACP, also known as Late Antiquity LIA, LALIA), Medieval Climate Anomaly (MCA), Little Ice Age (LIA) and Recent Warming) that most likely affected the annual duration of ice cover (i.e. ice phenology) in Spanish alpine lakes as it has been shown for the most recent phases (Sánchez-López et al., 2015). Ice phenology variability might have influenced differently the trace metal concentrations in LM sediments since the lake remains frozen about eight months per year (Sánchez-España et al., 2018). Direct atmospheric deposition of trace metal to the lake surface is hindered during cold periods when the lake is frozen and deposited metals would accumulate in the ice layer until discharged into the lake following ice melting. A similar process has been interpreted for pollen rain content during the late glacial and beginning of the Holocene (Leunda et al., 2017) as well as in other lakes in polar regions (Rodríguez-Pérez et al., 2019). In the case of mercury deposited on the ice and snow, it could also undergo re-emission to the atmosphere following heterogeneous photochemistry on the ice surface and/or snowpack (Angot et al., 2016). This process would release a fraction of the ice-trapped Hg back into the atmosphere contributing to lower atmospheric deposition of Hg to the

346 lake. On the contrary, large re-emission of other trace metals such as Pb, Cu, As and Zn
347 from ice lake surface is not expected since these elements are largely immobile and
348 would be remobilized during ice-melting and stored in the natural sink (i.e. the lake).
349 Additionally, trace metals deposition in the Southern Pyrenees mainly occurs during the
350 warm season when inland air masses enriched in trace elements and a thicker
351 atmospheric mixed layer occurs (Bacardit and Camarero, 2009). Ice phenology would
352 also affect the lake´s annual stratification patterns and thus trace metals mobility in the
353 water column. This process would affect Zn and, to a lesser extent, Cu and As (Sánchez-
354 España et al., 2018). Nevertheless, we do not expect that this seasonal process would
355 affect the annual depositional flux of these elements.
356
357 4.1.2 Principal Component Analyses of the geochemical dataset.
358
359 PCA applied over the geochemical dataset (trace metal concentration and accumulation
360 rates). PCA on trace metal concentration shows four main eigenvectors representing
361 81.84 % of the matrix variance (Table 2). These eigenvectors explain the main
362 environmental factors controlling sediment deposition and lake´s endogenic and
363 allochthonous processes. Factor loadings of each element in the extracted eigenvectors
364 (PCs) and PCs variability are shown in Figs. 3 and 4 and Fig. S1 highlighting the
365 fractionation of the communalities. Both PCA using trace metal concentration and
366 accumulation rates show similar variances and grouping of geochemical elements (Figs.
367 3 and S1; Tables 2 and S1).
368 The first component (PC1 46.7% of the variance) is related to lithogenic
369 elements (Zr, Sr, Si, Cr, Mg, Ti, B, K, Al and Ba) and represents the delivery of
370 allochthonous material to the lake via watershed run-off. Periods of increased run-off

371 occurred between 910-650 BCE, 160 BCE-30 CE, 660-830 CE and 1650-1770 CE most
372 likely related to periods with higher snow cover in winter and/or increase snowmelt in
373 summer. The second component PC2 (19,57 % of the total variance) is characterized by
374 large positive loadings of Hg (0,90) and Pb (0,77), and moderate positively loadings of
375 Cu (0,73), As (0,71), Cd (0,64) and Zn (0,59). PC2 suggest atmospheric deposition as
376 the main process controlling the sediment enrichment of PHTE. PC2 show relatively
377 low values during the IA while reached high values during the RP particularly between
378 60-200 yrs CE. PC2 strongly decreased during the EMA and progressively increased
379 since the onset of the HMA reaching maximum values at the end of the 19th century
380 (Fig. 4). PC2 progressively increased during the Little Ice Age when colder conditions
381 occurred in the Pyrenees (Morellón et al., 2012) suggesting climate influence on Hg
382 deposition since PC2 is dominated by Hg. Thus, increased Hg levels during the LIA
383 could result from lower re-emission of the Hg deposited on the snow/ice covering the
384 lake surface and the catchment and enhanced transfer to the sediment during thawing
385 events. Major increases in PC 1 and 2 show large temporal dissimilarities suggesting
386 that the main trace metal pollutants input by weathering and run-off are not the main
387 environmental processes driving hazardous trace metal pollutants in the lake.

388 The third component (PC3, 8.69% of the variance) is mainly characterized by
389 positive loadings of TOC, Fe and P and reflects the accumulation of organic matter in
390 the lake´s bottom and nutrients input. Recent limnological surveys in the lake
391 documented some variability in the biological activity in LM waters, although TOC
392 values in the water column are extremely low (ranging from 0.3 mg/L to 1.2 mg/L
393 (Sánchez-España et al., 2018)). Therefore, PC3 fluctuating values during the last 3000
394 years would therefore reflect the variability in lacustrine primary production. PC4 (6.88
395 % of the variance) is related to large positive loading of Ca, Mn and Cd. No carbonate

precipitates in the lake as the water column is undersaturated in calcite (Oliva-Urcia et al., 2018; Sánchez-España et al., 2018). Therefore, PC4 may reflect carbonate fluxes in the lake conditioned by the variable dissolution rate of carbonate particles from the watershed, controlled by water temperatures during the summer (Oliva-Urcia et al., 2018). Redox variability in the hypolimnion could also affect Mn and Cd as they are sensitive to redox-driven cycling in lacustrine systems (Hamilton-Taylor and Davison, 1995). PC4 shows relatively stable values suggesting that the lake has been well oxygenated during the last 3 millennia, similarly to recent years when limnological surveys have documented a well oxygenation of the lake´s water column throughout the annual cycle (Sánchez-España et al., 2018). PC4 peaks at 950 yrs BCE, 100 yrs BCE and 2000 yrs CE are more likely to respond to detrital carbonate accumulation in the lake since Mn is mostly linked to Ca-rich laminae in the Marboré sediments (Oliva-Urcia et al., 2018).

The moderate loadings of As and Zn in PCs 3 and 4 suggest that these elements can be either i) mobilized and re-precipitated in the sediment under anoxic/oxic changes in the hypolimnion and/or ii) fixed in organic compounds. Nevertheless, the continuous oxygenation of the hypolimnion and the very reduced biological activity (TOC in the sediment <1%) in this lake suggest that both factors do not have a significant influence on these elements variability during the Late Holocene. The lack of correlation between Hg and Pb with lithogenic and redox-sensitive elements and TOC also suggests that watershed runoff, redox variability and biological activity are not the main contributors to these major pollutant contents and fixation in the sediment. Therefore, although it may be a baseline deposition of some trace metals due to the weathering in the basin and run-off processes, the increase in PHTE would be mainly related to higher atmospheric deposition due to human activities at a local to subcontinental scale.

421

422 4.1.3 Temporal trace metal´s concentration evolution

423

424 Hazardous trace metals follow different down-core concentration evolutions in the
425 upper 175 cm of the analyzed sediment cores (Fig. 2). Pb concentration increased
426 progressively during the IA with mean [Pb] of 14.8 mg kg^{-1}. [Pb] abruptly increased at
427 the onset of the RP reaching maximum values between 50- 210 yrs CE. During this
428 period mean [Pb] of 46 mg kg^{-1} are above the Pb TEC (Threshold Effect Concentration)
429 guidelines in freshwater sediments (MacDonald et al., 2000), i.e. above the threshold
430 from which harmful effects on ecosystems are likely to be observed. Low [Pb] values
431 were recorded during the EMA and the HMA, with values of 19.6 mg kg^{-1} and 18.6 mg
432 kg^{-1} respectively, although [Pb] did not return to pre-roman values. Higher [Pb]
433 occurred during the LMA ([Pb] of 21.7 mg kg^{-1}) and the MP ([Pb] of 25.6 mg kg^{-1})
434 reaching the highest values during the IP, when [Pb] of 46 mg kg^{-1} resemble the Pb
435 values recorded during the RP. Arsenic showed increasing concentration values from the
436 onset of IA to the end of the RP reaching a maximum concentration peak of 11 mg kg^{-1}.
437 Then it progressively decreased until the end of the HMA and showed elevated and
438 fluctuating values during the MP and the IP with mean [As] of 10.8 mg kg^{-1} (above [As]
439 TEC values). Zn and Cu concentration progressively increased during the last 3000
440 years with mean values of 74.2 and 4.7 mg kg^{-1}, respectively. Mercury concentrations
441 remained low until the end of the Middle Ages (0.018 mg kg^{-1}), increased during the MP
442 (0,027 mg kg^{-1}) and doubled during the IP (0.054 mg kg^{-1}).

443

444 **4.2- Atmospheric transport of major pollutants.**

445 Air masses back trajectories reaching LM were computed to investigate the atmospheric
446 transport of main pollutants from the main mining districts in the Iberian Peninsula (Fig.
447 1). The analyses of back trajectories reaching LM reveal that 50 % of air masses come
448 from SW France and the Ebro valley (Table 1). Air masses sources progressively
449 decrease southward with Central and Western Spain contributing to 16.4 % of total air
450 masses in the region, Southern Spain (17.4 %) and Northern Africa (3 %). Air masses
451 from the Atlantic Ocean or emitted in the Central Iberian Peninsula are usually
452 displaced to the Western Mediterranean Sea due to the westerlies flows. Once in this
453 region, air masses can be trapped and funneled through the Ebro valley impacting in the
454 Pyrenean mountain range. Likewise, Northern African air masses reach the Western
455 Mediterranean basin and subsequently transported to the Pyrenees funneled through the
456 Ebro valley. Other pathways are possible, such as the direct arrival through the Iberian
457 Peninsula or, indirectly, through the Atlantic Ocean eventually reaching the Pyrenees
458 from the south. Air masses back trajectories indicate that the transport from emission
459 sources in central and southern Iberian Peninsula (e.g. Almadén, Rio Tinto, Cartagena,
460 Linares) is not direct and would follow the Western Mediterranean route.

461 On the other hand, changes in atmospheric patterns, particularly related to the
462 intensity of winds could have played an effect on delivery of trace metals from southern
463 Spain during past climate phases in the Late Holocene (Le Roux et al., 2012; Martínez
464 Cortizas et al., 2020; Sánchez-López et al., 2016). Indeed, the Roman Period
465 experienced an E-W humidity gradient marked by an interpaly between negative North
466 Atlantic Oscillation (NAO) and positive East Atlantic (EA) phases. These changes in
467 the atmospheric teleconnection patterns might result in different air masses trajectories

making different sources areas of metal pollution possible. Therefore, changes in the provenance of air masses is likely making alternative sources areas of metal pollution plausible. Inter-annual and multiannual variations in North Africa dust emissions have been extensively related to variability in atmospheric modes, such as the NAO and the ENSO (El Niño–Southern Oscillation) (Pey et al., 2013; Rodríguez et al., 2015; Salvador et al., 2014) when NAO positive phase occurs, the probability of transporting air masses from North Africa towards the IP is higher. Nevertheless, air masses travelling long distances usually move in upper layers, i.e. emissions from surface in the atmospheric boundary layer reach the free troposphere and then are transported by the westerlies flows. High altitude LM would therefore record the impact of long-range transport of trace metals-bearing air masses travelling in the free troposphere from southwestern Europe.

Global atmospheric Hg lifetime against surface deposition is estimated to be in the range of 3 to 6 months (Horowitz et al., 2017). Therefore, it is very likely that major Hg extractive episodes in Almadén resulted in high deposition in LM area. Indeed, 9.5% of the total back-trajectories arriving to LM pass over Almadén region (Table 1). Regarding other more immobile elements such as Pb, Zn, As or Cu, several studies have quantified the modern atmospheric transport of PHTE related to mining operations to determine how far the pollutants could travel from the emission sources (Asif et al., 2018; Csavina et al., 2012). These investigations documented the exponential fall of As, Zn and Pb concentration values with the distance from the mining site. Residence times of mining related-atmospheric particles might be limited to hours when PHTE would travel hardly beyond a few dozens of km except for minimum quantities. Several ore deposits are located within this distance to LM, as the Spanish Ag, Pb and Cu mines from Bielsa and Benasque and the French Montaigu mines, where Ag and Pb have been

493 exploited in ancient times (Calvo, 2008; Girard et al., 2010; Pérez et al., 2008). Ore
494 extraction in larger Ag-Pb and Cu Pyrenean mines such as Arditurri or Banca, in the
495 Basque Country and Southwestern France respectively has also been documented since
496 Roman times (Ancel et al., 2001; Thalacker, 1804). Nevertheless, back trajectories
497 results demonstrate that the emissions from large-scale mining districts located in
498 Southern Spain can easily reach LM in less than three days (Fig. 1) depositing PHTE in
499 the lake. Indeed, Rio La Carolina-Linares, Mazarrón-Cartagena and Río Tinto mines
500 source areas represent 8.5, 8.4 and 7 % respectively. Therefore, the few air masses from
501 the southern mining districts could rapidly transport the metals emitted during metal
502 extraction activities and being eventually recorded in LM sedimentary archive.
503
504 **4.3- Sources and environmental impact variability of mercury, silver, lead and**
505 **copper mining**
506
507 4.3.1 Lead
508
509 Positive Pb EF was found during several periods of the last 3000 years (Fig. 4). Pb EF
510 and Pb_{flux} remained low until 700 BCE and progressively increased since then until a
511 maximum in 460 yrs BCE (Pb EF 2, Pb MAR 12.7 X 10^3 µg m^2 yr^{-1}) and progressively
512 decrease afterwards. Pb EF peaked again at 140 BCE (Pb EF 1.8, Pb MAR 20.6 X 10^3
513 µg m^2 yr^{-1}). Maximum Pb EF was found during the RP between 20 and 375 yrs CE (Pb
514 EF 3.5, Pb MAR 31 X 10^3 µg m^2 yr^{-1}). Maximum peaks occurred at 50 yrs CE (Pb EF
515 4.5, Pb MAR 37.5 X 10^3 µg m^2 yr^{-1}) and 180 yrs CE (Pb EF 5, Pb MAR 38.5 X 10^3 µg
516 m^2 yr^{-1}). Pb EF progressively decreased since the end of the RP reaching minimum
517 values similar to natural baseline conditions between 750-870 yrs CE. Pb EF increased

518 at the onset of HMA at 950 yrs CE and remained high (mean values of 1.6) until 1350
519 yrs CE (Pb EF 1.8, Pb MAR 15 X 10^3 µg m^2 yr^{-1}). Low Pb levels occurred between
520 1500 and 1820 yrs CE (Pb EF 1.5, Pb MAR 17.5 X 10^3 µg m^2 yr^{-1}) reaching minimum
521 enrichment (1.1) at 1700 yrs CE that resembles natural background values. During the
522 IP Pb EF was very high (Pb EF 4.1, Pb MAR 39.3 X 10^3 µg m^2 yr^{-1}) with maximum
523 values at 1880 yrs CE (Pb EF 6.3, Pb MAR 51.2 X 10^3 µg m^2 yr^{-1}). As and Zn follows
524 the same trend than Pb suggesting a common source since both elements are by-
525 products of ore exploitations from local veins enriched in galena, fluorite and sphalerite
526 minerals
527
528 *4.3.1.1 Iron Age*
529
530 The Pb isotopic dataset show a large variability across a well-defined mixing line (Fig.
531 5). $^{208}Pb/^{206}Pb$ and $^{207}Pb/^{206}Pb$ ratios show the lowest (geogenic) values during the IA
532 thus suggesting that Pb concentrations during this interval may reflect natural sources.
533 Small increases in Pb EF during the 6th and 3rd centuries BCE may reflect ore extraction
534 from the region of Murcia in Spain (Cartagena/Mazarrón mines) in agreement with
535 previous archaeological and paleolimnological findings from coastal lagoons in Western
536 Mediterranean that recorded the environmental impact related to the intense mining
537 activities in the Cartagena mining district (Elbaz-Poulichet et al., 2011; Manteca et al.,
538 2017).
539
540 *4.3.1.2 Roman Period*
541

The large increase in Pb during the Roman Empire also coincides with the highest (anthropogenic) $^{208}Pb/^{206}Pb$ and $^{207}Pb/^{206}Pb$ isotopic ratios. The agreement of the isotopic values between 50 and 375 CE and the isotopic Pb signature from local high-altitude ore deposits from nearby mines (i.e. Parzán, Bizielle, Cierco, Palouma) might suggest the exploitation of Pb and Ag in high alpine environments in the Central Pyrenees during the Roman Period. $^{208}Pb/^{206}Pb$ and $^{207}Pb/^{206}Pb$ isotopic ratios during the RP are similar to those during the turn of the last century when Parzán mines were largely exploited (Fanlo et al., 1998; Nieto-Callen, 1996), suggesting a plausible Roman exploitation of these mines. Nevertheless, in spite of the geochemical similarities of LM signatures for Roman and recent mining compared to regional sites, the LM isotope signatures do not allow a clear adscription to local PHTM mining sources since we cannot disentangle local and regional mining from other regional pollution sources.

In our opinion, the anomalously high Pb levels during the Roman Empire imply that most of the trace metal pollution came from large-scale regional mining rather than local sources. Several indicators suggest that the exploitation of ore resources in high alpine areas from the Southern Central Pyrenees would have remained very local (if any) resulting in very reduced metal smelting and associated pollution during this period:

i) The absence of historical records documenting Roman mining in this region. Indeed, Roman mining is often associated to the development of large infrastructures to favor transport of metal resources which are not known in the area. As an example, Arditurri silver mines exploitation during roman times come with the development of large associated infrastructures for trading (Irabien et al., 2012; Urteaga, 2014).

ii) Mining procedures used in these exploitations required a continuous supply of goods for metal roasting and smelting which frequently results in large regional environmental impacts (i.e. deforestation and fires) (Pèlachs et al., 2009). Such environmental impacts (i.e. pollen indicators of deforestation, major increases in charcoal as indicator of biomass burning) have not been documented in regional and local paleoenvironmental reconstructions (González-Sampériz et al., 2017; Leunda et al., 2017; 2020) (Fig. 6). Additionally, studies in charcoal kilns from high altitude areas of the Pyrenees documented that charcoal production for ore smelting was likely very localized in time and space (Pèlachs et al., 2009).

A unique feature of the LM Pb record compared to other Pyrenean records is that the maximum pre-industrial Pb occurred during the Roman period, synchronous to an alpine peatbog record from Northern Central Pyrenees (Hansson et al., 2017), but not with other sites in Eastern and Western Pyrenees, where maximum Pb levels appeared later at 660-680 yrs CE (Camarero et al., 1998; Irabien et al., 2012). The anomalously high Pb concentration in LM and the absence of large mining operations in the Central Pyrenees suggest that most of the trace metal pollution came from other large-scale regional mining sources. Southern Spain hosts the most important Ag and Pb mines from the Ancient World. It has been calculated that about 70% of the total atmospheric Pb released to the environment during Roman times worldwide could be assigned to the Rio Tinto and Mazarrón source areas (Rosman et al., 1997). Therefore, increased Pb fluxes during the RP might reflect the signal of large-scale mining in southern Spain. Indeed, the isotope values of LM samples for the last 3000 years fall along a mixing line between two main end-members defined by Mazarrón-Cartagena and Rio Tinto mining districts. Those LM samples from the IA show mostly a composition similar to

591 Mazarrón-Cartagena mining district, while isotopic values during the RP have a larger
592 range that could be an indication of more varied sources during that time, including a
593 higher influence of Rio Tinto as well as higher input of lead from the lake´s watershed
594 via run-off. Northwestern Spain would also constitute alternative metal pollution
595 sources since mining activities have been well documented in the area (Martínez-
596 Cortizas et al., 2013). Nevertheless, their contribution to the Lake Marboré Pb record
597 are expected to be very reduced.

598 The environmental impact of Roman mining has also been detected in other
599 natural archives in the French Pyrenees, and Northwestern and Southern Spain (e.g
600 (García-Alix et al., 2013; Hanebuth et al., 2018; Hansson et al., 2017; Hillman et al.,
601 2017; Kylander et al., 2005; Manteca et al., 2017; Martín-Puertas et al., 2010; Martínez-
602 Cortizas et al., 1997; 2013; Pontevedra-Pombal et al., 2013)). Nevertheless, those
603 records show variable timing and magnitude due to their location with respect to the
604 emission sources. Thus, while LM Pb record agrees very well with Pb levels recorded in
605 peatbogs from the Northern Central Pyrenees (Hansson et al., 2017) (Fig. 6) as well as
606 with Pb levels recorded in coastal sediments from NW Mediterranean (Portlligat bay,
607 270 km east from LM) (Serrano et al., 2011). In the other hand, Pb levels in Lake Zoñar
608 (Southern Spain) showed maximum values between 500 and 100 yrs BCE due to
609 extensive mining in Southern Iberian Peninsula by Iberians, already influenced by
610 Greeks and Phoenicians (Fig. 6) (Martín-Puertas et al., 2010). Further timing
611 discrepancies have been found with other high-altitude pollution and remote records in
612 the Alps (Cold du Dome ice core Western Alps (Preunkert et al., 2019)) and Greenland
613 (NGRIP2 (McConnell et al., 2018)) (Fig. 6). This asynchrony in maximum Pb levels
614 underlines the variable influence of diverse emission sources in each location.
615 Greenland ice core records would represent the whole European emissions and Western

Alps ice cores would record mostly emissions from France and Northern Mediterranean. On the other hand, LM would record PHTM emissions mostly from the main mining districts from Southwestern Europe representing the atmospheric Pb levels during the RP at a regional to sub-continental scale because of the privilege location of LM in the free troposphere. Indeed, the high Pb content in the atmosphere was a major health concern in the Iberian Peninsula during Roman times affecting Iberian population as recorded in the Pb isotopic composition of human bones from living individuals in NW Iberian Peninsula (López-Costas et al., 2020).

Pb concentrations and $^{208}Pb/^{206}Pb$ and $^{207}Pb/^{206}Pb$ isotopic ratios progressively declined since the end of the 2nd century CE coinciding with the decrease of Roman mining in the Iberian Peninsula, largely attributed to the socio-economic crises of the Roman Empire. These economic crises started with the Antonine plague that disrupted mining through high mortality and decreased demand as well as with the reduced silver content used in coinage in the 3rd century CE (McConnell et al., 2018). During EMA, the proximity of the mines to population settlements was a significant factor for mine abandonment due to the transportation costs and because local miners adopted methods and infrastructure less efficient than those of Roman times (Martinon-Torres and Rehren, 2011).

4.3.1.3 Last millennium

An increase in Pb EF and MAR and a shift towards more radiogenic values occurred during the HMA and LMA most likely related to the renew mining activities and the exploitation of more local mines as Parzán (Fig. 1). This period coincides with widespread innovations in mining and refining processes in Europe to reach the high

641 demands of the increasing European population between 11-13th centuries. The Pb peak
642 at the second half of the 12th century coincides with the first historical evidences of local
643 mining in Parzán when Aragonese King Alfonso II conceded official privileges of
644 exploitation of the Bielsa mines to the local people (Bielza de Ory, 1983). The decline
645 of Pb levels since 1350 CE recorded in LM sediments coincides with the interrupted
646 metal production in Europe during the Black Death Pandemic (1349-1353 yrs CE) that
647 dropped atmospheric Pb to undetectable levels (More et al., 2017). Pb levels recovered
648 afterwards, but remained low during the following centuries might be related to the
649 onset of large-scale silver mining in South America. In this context, high alpine, small-
650 scale silver mines such as the ones in the Axial Pyrenees were less profitable and
651 probably intermittently abandoned. However, historical archives documented that more
652 than 15000 kg of Pb were produced (and smelted in local kilns) in Parzán by the end of
653 the 16th century (Nieto-Callen, 1996). Only at the end of the 19th century, Pb levels
654 increased exponentially in LM (Fig. 6) and other Pyrenean lakes (Corella et al., 2017;
655 2018) due to large-scale exploitation of Parzán mines (Fanlo et al., 1998; Nieto-Callen,
656 1996).

657 The correspondence between atmospheric Pb levels and warmer climate phases
658 during the last millennium suggests a connection between source availability (i.e. ore
659 extraction and smelting) and depositional processes with climate. Thus, the Pb and Ag
660 mining extractive period in the Pyrenees during the HMA and LMA coincided with the
661 MCA, a warm and arid period in the Iberian Peninsula between 950 and 1350 yr CE
662 (Moreno et al., 2012). Prolonged snow-free periods at the mining sites would have
663 favoured ore resources exploitation in mountain areas. On the other hand, a return to
664 almost baseline natural backgrounds of atmospheric Pb levels that occurred between the
665 EMA and the MP coincided with the DACP and the LIA, known as cold periods in NE

Iberian Peninsula (Corella et al., 2012; 2013; Morellón et al., 2012) and Iberian mountains (Oliva et al. 2018). Atmospheric pollution levels were particularly low during the Maunder Minimum (1645-1715 yrs CE) when trace metals accumulation fluxes were greatly reduced (Fig. 4). Therefore, climate variability has been likely also a determinant factor controlling mining in high-alpine environments (e.g. Parzán mines located at > 2300 m a.s.l.) during the last centuries. The relation between past warmer climate phases and mining activities in high alpine environments was also observed in the western Alps (Guyard et al., 2007) where ore extraction became possible because of glaciers retreated in the region when temperature increased.

4.3.2 Copper

Cu EF increased progressively reaching the highest values at the end of the IA at 360 yrs BCE (Cu EF 2) (Fig. 4). Cu EF decreased during the first phase of the RP until 50 yrs CE. Cu EF started to increase during the mid 4th century and peaked at the onset of the 5th century CE (410 yrs CE, Cu EF 3.2). Cu EF reduced during the EMA and increased during the HMA and LMA (Cu EF 2) with maximum Cu enrichment at 1200 yrs CE (Cu EF 2.7). Cu EF remained high during the 16th century with mean Cu enrichment of 2.4. Cu EF decreased during the 18th century and increased again during the IP (Cu EF 2.6) peaking at the turn of the 19th century (Cu EF 3.4).

The first documented increase in copper concentrations in Greenland exceeding the natural levels occurred about 2500 years ago (Hong et al., 1996) and provides evidence for widespread copper mining during the Iron Age. The oldest presence of copper miners and metalworkers in the region was documented in the Montpellier region (Southern France) in the 3rd millennium BCE (Ambert et al., 2002) while large

691 copper mines were in operation in N Iberia since the Chalcolithic (De Blas, 2005; Vidal,
692 2012; Martínez-Cortizas et al., 2016)

693 The Cu enrichment in LM during the 4th century BCE agrees well with an
694 enrichment in Cu recorded in peatbogs sediments from Northern Central Pyrenees
695 between 480–180 yrs BCE (Hansson et al., 2017) suggesting copper mining from the
696 abundant Cu-rich ore deposits in the region (Calvo, 2008). The high Cu levels since 50
697 yrs CE remained elevated during almost all Roman Empire most likely due to the highly
698 polluting smelting technologies used for copper production during Roman times in
699 Europe (Hong et al., 1996). This is in agreement with the roman exploitation of Banca
700 mines (French Western Pyrenees), the largest roman copper mines in France, between
701 1st century BCE and 4th century CE (Ancel et al., 2012; Urteaga, 2014). Nevertheless,
702 the highest copper production in the Iberian Peninsula occurred in the Río Tinto region
703 (SW Iberia) as well in other copper mines from NW Iberia (Wilson, 2002). Maximum
704 atmospheric Cu levels between the mid 4th century and the early 5th century might
705 reflect the increase in copper demand for coinage when Roman monetary system shifted
706 to a bimetallic currency composed of a gold and copper alloy (McConnell et al., 2018;
707 Wilson, 2002).

708 Copper levels increased again in LM record at around 1200 yrs CE and persisted
709 high for almost five centuries. The enrichment in the early 13th century occurred almost
710 one century before the first historical documents of copper mining in the area when
711 kings Alfonso II and Jaime II conceded privileges for mineral extraction to local
712 noblemen in the Pyrenean surrounding valleys as well as from Santa Eulalia la Mayor
713 (60 km south of LM) in 1277 and 1293 yrs CE, respectively. The use of local kilns for
714 Cu, Ag, Pb and Fe smelting practices were also documented during this time (Nieto-
715 Callen, 1996). Cu levels decreased during the 18th century and peaked again in the 19th

716 century. This variability is in agreement with the historical local mining activities of the
717 area that derived, on the one hand, in unsuccessful copper resources prospection during
718 the 18th century and, on the other hand, the boost of copper mines in the region during
719 the 19th century (Nieto-Callen, 1996).
720
721 4.3.3 Mercury
722
723 Hg levels in LM showed a significant variability during the Late Holocene. Mercury EF
724 and Hg_{flux} were at the lowest levels until 620 yrs BCE (EF <1, 12.8 µg m^2 yr^{-1}) and
725 remained high between 620–270 yrs BCE (Hg EF=1.2, Hg MAR=13.4 µg m^2 yr^{-1}). Low
726 values were found until 20 yrs CE and then increased slightly increase during the RP.
727 Hg EF remained stable until the MP, when Hg EF progressively increased with mean
728 Hg EF values of 1.9 (Hg MAR=18,4 µg m^2 yr^{-1}) reaching maximum values during the
729 IP (Hg EF=3.7, Hg MAR=40 µg m^2 yr^{-1}).
730 Hg emissions before the Industrial Period have been mostly attributed to
731 historical mining, volcanic activity and coal burning (Cooke et al., (2020) and
732 references therein). Periods of Hg levels in LM are not coherent with the impact of the
733 main volcanic eruptions in the Northern Hemisphere, although the decadal
734 chronological resolution of LM might have hindered the identification of volcanic
735 episodes with large Hg emissions to the atmosphere (e.g. Vesubio volcanic eruption in
736 79 CE coinciding with the higher Hg EF during the 1st century CE). Recent studies in
737 the French Pyrenees and Southeastern France have suggested that atmospheric Hg
738 deposition increase during the Medieval and the Modern Period was mostly caused by
739 enhanced Hg emissions from biomass burning (Elbaz-Poulichet et al., 2011; Enrico et
740 al., 2017). Nevertheless, Hg MAR and EF in LM does not coincide with major

741 deforestation and burning episodes in alpine environments from the Southern Central
742 Pyrenees (González-Sampériz et al., 2017; 2019; Leunda et al., 2017; 2020) (Fig. 6).
743 Therefore, Hg net fluxes recorded in LM would most likely be related to Hg emissions
744 caused by local and/or regional mining activities.

745 Hg EF for the period 1000 BCE-1500 CE correlates well with Zn EF (σ=0,81)
746 and, to a lesser extent, with Cu (σ=0,65). This correlation suggests that Hg enrichments
747 before the Modern Period might be related to the exploitation of i) local Pb (Ag)-Zn
748 veins which are dominated by galena and sphalerite deposits (Subías et al., 2015) and/or
749 ii) chalcopyrite exploited in local fire settings for copper extraction since these minerals
750 can host significant Hg concentrations (George et al., 2018; Rytuba, 2003) which can
751 eventually result in increased Hg emissions (as by-products) to the local atmosphere.
752 Recent paleolimnological studies in the Alps have also highlighted the influence of local
753 Cu and Pb-Ag ore exploitations controlling Hg enrichment in high alpine environments
754 in ancient times (Elbaz-Poulichet et al., 2020). Nevertheless, we cannot exclude Hg
755 emissions from regional sources (i.e. Almadén mines, Central Spain) since large-scale
756 cinnabar mining in Almadén has been carried out during the last 2500 years (Hernandez,
757 2007). Considering back trajectories analyses and atmospheric Hg residence times it is
758 very likely that major Hg extractive episodes in Almadén resulted in an increase Hg
759 accumulation in LM. Almadén´s mining exploitation by Romans and Arabs resulted in
760 large Hg release to the atmosphere. Indeed, the Roman writer Pliny the Elder wrote
761 about the extraction of Hg (and its distillation in marmites) and its trade between Spain
762 and Rome in the 1st century CE, while the Arabs intensified Hg production in Almadén
763 with more than 1000 laborers working in the mines during the 11th century (Goldwater,
764 1972).

765 The progressive increase in Hg EF and MAR that occurred in LM during the last
766 500 years greatly differs from the other metal EFs evolution (Fig. 7) and follows the Hg
767 historical production in Almadén documented during the last five centuries (Hylander
768 and Meili, 2003). Hg production significantly increased in the 16th century due to the
769 need for Hg amalgamation in silver mining in the Spanish colonies. As a result, large
770 amounts of Hg dissipated to the environment. As an example, between 1571 and 1660
771 yrs CE approximately 25000 tons of Hg were produced in the mines (Hylander and
772 Meili, 2003). This likely resulted in a 30% increase in Hg MAR during this period (18.2
773 µg m^2 yr^{-1}) from the stable Hg MAR before the Modern Period (13.7 µg m^2 yr^{-1}). A 25
774 % decrease in Hg MAR at 1675 yrs CE could be explained by the drastic decrease in Hg
775 Almadén production during the second half of the 17th century due to the exhaustion of
776 Hg resources in Almadén (Bethell, 1984) and the reduction of Hg shipping to South
777 America. Nevertheless, the discovery of new veins in Almadén at the turn of the century
778 most likely explains the abrupt increase in Hg MAR during the early 18th century (22.6
779 µg m^2 yr^{-1}). Hg levels progressively increased during the Industrial period peaking at
780 the turn of the 20th century (EF of ~4 and MAR of ~40 µg m^2 yr^{-1}) and between 1960-
781 1970 CE (EF of 4.8 and MAR 70 µg m^2 yr^{-1}) when Hg production peaked at 10 000 tons
782 per year (Hylander and Meili, 2003). The Hg variability pattern recorded in LM during
783 the 20th century is similar to the recent Hg variability highlighted in multi-short cores
784 studies in Southern Sweden and NW Spain (Bindler et al. 2004; Martínez-Cortizas et
785 al., 2012).
786 The 2-fold decline in Hg MAR since 1970 CE coincides with a decreasing trend in Hg
787 production in Almadén during the last decades (Fig. 7) until its closure in the 2000s.
788 This 2-fold decrease in atmospheric Hg concentrations since the 1970s is in agreement
789 with direct atmospheric monitoring and glacier firn records (*EMEP; Faïn et al., 2009*).

In the Iberian Peninsula, anthropogenic Hg release to the atmosphere due to mining activities in Almadén ca. 2500 years before present was first documented in peat cores from NW Spain (Martinez-Cortizas et al., 1999), estuarine sediments from Southwestern Spain (Leblanc et al., 2000) and marine sediments in the Western Mediterranean (Portlligat Bay) (Serrano et al., 2013). In the Pyrenees, atmospheric Hg fluxes have been previously reported in peat sediments from the French Pyrenees (Enrico et al., 2017) as well as in lake Montcortès in the Pre-Pyrenees located at 1031 m a.s.l. (Corella et al., 2017). LM Hg concentration and fluxes agree well with atmospheric Hg fluxes previously reported in peat sediments from the French Pyrenees (Enrico et al., 2017) as well as in low-elevation lake Montcortès sediments in the Pre-Pyrenees (Corella et al., 2017) highlighting the regional to sub-continental scale pollution recorded in these natural archives.

5- SUMMARY AND CONCLUSIONS

The geochemical Lake Marboré record allowed us to understand the atmospheric variability of hazardous trace metals related to historical mining and metalworking activities in the Iberian Peninsula during the Late Holocene. The location of the lake at 2600 m a.s.l. makes it particularly sensitive to tropospheric transport of trace metals. Historical metallurgy has derived in a significant increase in Hg, Pb and, to a lesser extent, Zn, Cu and As during the Pre-Industrial Period constituting one of the oldest, large-scale anthropogenic impact on the environment. This historical atmospheric pollution has left a profound geochemical signature in the lake where several trace metals reach concentration levels that might have had ecotoxicological implications in these high-mountain ecosystems.

The multidisciplinary approach involving statistical, isotopic and meteorological re-analyses have also enabled the reconstruction of the history and sources of hazardous trace metal pollutions over the last 3000 years. Back trajectories analyses show that air masses capable of transporting atmospheric pollutants to Lake Marboré may come from almost all southwestern Europe and northern Africa in less than 3 days highlighting the sensitiveness of the lake to track environmental pollution sources at a local to sub-continental scale. Pb isotopic analyses suggest that Ag and Pb mining in South-eastern Spain might have been responsible for subtle trace metal enrichment during the Late Iron Age. Very high atmospheric Pb fluxes were found during the Roman Empire most likely related to the global rise of atmospheric Pb emission from Río Tinto and Mazarrón mines emplaced in Southern Iberia Peninsula. Isotope analyses suggest a contribution of small-scale ore exploitation from local, high-altitude mines but more archaeological surveys are needed as the assessment of all local sources is a critical issue when reconstructing the history of pollution using natural archives. Independently of the source we find evidence that atmospheric Pb levels were of the same magnitude that the ones found during the Industrial Period. Local Ag, Pb and Cu mining reactivated in the Central Pyrenees during the High Middle Ages when socio-economic conditions and mild-climates allowed ore extraction in high-alpine environments and all over the Iberian Peninsula. These local mining activities significantly decreased during the harsh climate conditions documented at the onset of the Little Ice Age. Contrarily, atmospheric Hg progressively increased during the Modern Period due to the large-scale production in Almadén mines in Central Spain, leading to high loads of Hg burden in Pyrenean sedimentary environments.

Lake Marboré record of past emissions related to mining and metalworking activities shows a common pattern with other European pollution records showing a

climax during the Roman period, Medieval times and since the Industrial Revolution. This agreement could be partly explained by the location of the lake above the mixing atmospheric boundary layer, therefore, recording long-range (inter-hemispheric) atmospheric pollutants transport. The lake´s location in a high elevation area, as well as the watershed and limnological characteristics of Lake Marboré makes this site a unique record of past atmospheric contamination that highlights the usefulness of long-term pollution archives to contextualize current atmospheric pollution levels. Indeed, the environmental consequences and atmospheric Pb pollution in Antiquity are substantial and could even exceed present-day levels.

This study provides a further understanding of the pollution burden legacy in lacustrine sediments constitutes a significant environmental hazard for high-mountain ecosystems that should be adequately quantified and monitored. Our findings also contribute to the contextualization of current air metal pollution by reconstructing long-term (centennial to millennial-scales) atmospheric trace metal levels beyond the very few instrumental measurements that barely spans the last decades. Nevertheless, the determination of pollution sources presented in this study are not entirely conclusive. Follow-up studies on Lake Marboré focussed on Hg, Pb, Nd and Sr isotopes will shed more light on the provenance and biogeochemical cycling of the main pollutants deposited in the lake.

6- ACKNOWLEDGMENTS

Financial support has been received by the Sobrarbe Geopark through the project "Reconstrucción de la minería histórica en la Comarca del Sobrarbe y su impacto ambiental durante el Antropoceno") and by the Spanish Ministry of Economy and

Competitiveness (MINECO) project MEDLANT (CGL2016-76215-R). This work is also supported by the FEDER funds through the INTERREG V-A Spain-France-Andorra (POCTEFA 2014-2020, REPLIM project, Ref. EFA056/15).

7- FIGURE CAPTIONS

Fig. 1: Frequency map of air mass back trajectories arriving to Lake Marboré (LM, blue circle). Yellow triangles indicate the location of historical mining sites mentioned in the text (1- Parzán; 2- Banca; 3- Arditurri; 4- Emporion; 5- Almadén; 6- Rio Tinto; 7- La Carolina-Linares; 8- Mazarrón-Cartagena).

Fig. 2: LM down-core evolution of Potential Harmful Trace Metal (PHTM) and aluminum concentrations, Organic Matter Content (TOC) and sediment density values.

Fig. 3. Communalities of the geochemical elements obtained from Principal Component Analyses (PCA).

Fig. 4. Principal Components eigenvectors (PC) and Enrichment factors (EF) and normalization (coloured area) of PHTM recorded in LM during the last 3000 years. Main historical periods are also indicated; Iron Age (IA), Roman Period (RP); Early, High and Late Middle Ages (EMA, HMA and LMA respectively); Modern Period and beginning of Contemporary Age (MP); Industrial Period (IP).

Fig. 5. Changes in $^{208}Pb/^{206}Pb$ and $^{207}Pb/^{206}Pb$ isotopic ratio in LM compared with other natural and anthropogenic (mining) sources. Different Pb isotopic values have been obtained from: Oxford archeological lead isotope database (OXALID) (Stos-Gale and Gale, 2009) for the Linares, Rio Tinto and Cartagena mines, Arditurri mines (Velasco et al., 1996), local galena mines from Emporion (NE Spain) (Montero-Ruiz et al., 2007),

ore deposits and local mines from Southern Central Pyrenees (Camarero et al., 1998; Girard et al., 2010; Subías et al., 2015).

Fig. 6. From bottom to top: Lead enrichment factor (EF), Pb Mass Accumulation Rates (MAR) during the last 3000 years; Calcite sublayering in Lake Montcortès as a proxy of prolonged winter conditions in Southern Central Pyrenees (Corella et al., 2012); Charcoal fluxes in LM and Lake Basa de la Mora sediment records as proxies of fires and human activities in the area (Leunda et al., 2020); Pb isotopic ratios in LM; Etant Mort Pb EF (redrawn from Hansson et al., (2017)); Lead content in western Alps (Col du Dome ice core (Preunkert et al., 2019)) and Greenland ice cores (McConnell et al., 2019). Coloured vertical bars represent the main climatic phases during the Late Holocene.

Fig. **7.** Atmospheric mercury (Hg) deposition in the Central Pyrenees over the last millennium from LM (this study) and Montcortès (Corella et al., 2017) as well as estimations of mercury production in Spanish mines (Hylander and Meili (2003)). Main historical and climatic phases are also indicated.

8- REFERENCES

Ambert. P.. Coularou. J.. Cert. C.. Guendon. J.-L.. Bourgarit. D.. Mille. B.t.. Dainat. D.. Houlès. N.. Baumes. B.. 2002. Le plus vieil établissement de métallurgistes de France (IIIe millénaire av. J.-C.): Péret (Hérault). Comptes Rendus Palevol 1. 67-74.

Amos. H.M.. Sonke. J.E.. Obrist. D.. Robins. N.. Hagan. N.. Horowitz. H.M.. Mason. R.P.. Witt. M.. Hedgecock. I.M.. Corbitt. E.S.. 2015. Observational and modeling constraints on global anthropogenic enrichment of mercury. Environmental Science & Technology 49. 4036-4047.

912 *Ancel. B.. Dardignac. C.. Parent. G.. Beyrie. A.. 2001. La mine de cuivre antique*
913 *des Trois Rois à Banca. vallée de Baïgorry (Pyrénées-Atlantiques). Sablayrolles éd.*
914 *179-194.*

915 *Ancel. B.. Parent. G.. Beyrie. A.. Kammenthaler. E.. Dardignac. C.. 2012.*
916 *Stratégie d'exploitation et galerie d'exhaure dans la mine de cuivre antique de Banca*
917 *(Pyrénées Atlantiques). L'eau: usages. risques et représentation dans le Sud-Ouest de la*
918 *Gaule et le Nord de la péninsule Ibérique. de la fin de lÂge du Fer à l'Antiquité tardive*
919 *21. 169-189.*

920 *Angot. H.. Dastoor. A.. De Simone. F.. Gårdfeldt. K.. Gencarelli. C.N..*
921 *Hedgecock. I.M.. Langer. S.. Magand. O.. Mastromonaco. M.N.. Nordstrøm. C.. 2016.*
922 *Chemical cycling and deposition of atmospheric mercury in polar regions: review of*
923 *recent measurements and comparison with models. Atmospheric Chemistry & Physics.*
924 *16. 10735–10763.*

925 *Appleby. P.G.. 2001. Chronostratigraphic techniques in recent sediments. In:*
926 *Last. W.M.. Smol. J.P. (Eds.). Tracking Environmental Change Using Lake Sediments.*
927 *Volume 1: Basin Analysis. Coring. and Chronological Techniques. Kluwer Academic*
928 *Publishers. Dordrecht. pp. 171-203.*

929 *Asif. Z.. Chen. Z.. Han. Y.. 2018. Air quality modeling for effective environmental*
930 *management in the mining region. Journal of the Air & Waste Management Association*
931 *68. 1001-1014.*

932 *Bacardit. M.. Camarero. L.. 2009. Fluxes of Al. Fe. Ti. Mn. Pb. Cd. Zn. Ni. Cu.*
933 *and As in monthly bulk deposition over the Pyrenees (SW Europe): the influence of*
934 *meteorology on the atmospheric component of trace element cycles and its implications*
935 *for high mountain lakes. Journal of Geophysical Research: Biogeosciences 114.*

Bacardit. M.. Camarero. L.. 2010. Modelling Pb. Zn and As transfer from terrestrial to aquatic ecosystems during the ice-free season in three Pyrenean catchments. Science of the Total Environment 408. 5854-5861.

Bacardit. M.. Krachler. M.. Camarero. L.. 2012. Whole-catchment inventories of trace metals in soils and sediments in mountain lake catchments in the Central Pyrenees: apportioning the anthropogenic and natural contributions. Geochimica et Cosmochimica Acta 82. 52-67.

Bethell. L.. 1984. Colonial Latin America. Cambridge University Press.

Bielza de Ory. V.. 1983. Estudio histórico geográfico del Valle de Bielsa.". Colección.

Biester. H.. Bindler. R.. Martinez-Cortizas. A.. Engstrom. D.R.. 2007. Modeling the past atmospheric deposition of mercury using natural archives. Environmental Science & Technology 41. 4851-4860.

Bindler. R.. Klarqvist. M.. Klaminder. J.. Förster. J.. 2004. Does within-bog spatial variability of mercury and lead constrain reconstructions of absolute deposition rates from single peat records? The example of Store Mosse. Sweden. Global Biogeochemical Cycles. 18(3).

Boës. X.. Rydberg. J.. Martinez-Cortizas. A.. Bindler. R.. Renberg. I.. 2011. Evaluation of conservative lithogenic elements (Ti. Zr. Al. and Rb) to study anthropogenic element enrichments in lake sediments. Journal of Paleolimnology 46. 75-87.

Calvo. M.. 2008. Minerales de Aragón. Prames. Zaragoza.

Camarero. L.. 2003. Spreading of trace metals and metalloids pollution in lake sediments over the Pyrenees. Journal de Physique IV (Proceedings). EDP sciences. pp. 249-253.

961 *Camarero. L.. 2017. Atmospheric chemical loadings in the high mountain:*
962 *current forcing and legacy pollution. High Mountain Conservation in a Changing*
963 *World. Springer. Cham. pp. 325-341.*

964 *Camarero. L.. Masqué. P.. Devos. W.. Ani-Ragolta. I.. Catalan. J.. Moor. H.C..*
965 *Pla. S.. Sanchez-Cabeza. J.A.. 1998. Historical Variations in Lead Fluxes in the*
966 *Pyrenees (Northeast Spain) from a Dated Lake Sediment Core. Water. Air. and Soil*
967 *Pollution 105. 439-449.*

968 *Cooke. C.A.. Balcom. P.H.. Kerfoot. C.. Abbott. M.B.. Wolfe. A.P.. 2011. Pre-*
969 *Colombian mercury pollution associated with the smelting of argentiferous ores in the*
970 *Bolivian Andes. Ambio 40. 18-25.*

971 *Cooke. C.A.. Martínez-Cortizas. A.. Bindler. R.. Gustin. M.S.. 2020.*
972 *Environmental archives of atmospheric Hg deposition–A review. Science of the Total*
973 *Environment 709. 134800.*

974 *Corella. J.. Saiz-Lopez. A.. Sierra. M.. Mata. M.. Millán. R.. Morellón. M..*
975 *Cuevas. C.. Moreno. A.. Valero-Garcés. B.. 2018. Trace metal enrichment during the*
976 *Industrial Period recorded across an altitudinal transect in the Southern Central*
977 *Pyrenees. Science of the Total Environment 645. 761-772.*

978 *Corella. J.P.. Brauer. A.. Mangili. C.. Rull. V.. Vegas-Vilarrúbia. T.. Morellón.*
979 *M.. Valero-Garcés. B.L.. 2012. The 1.5-ka varved record of Lake Montcortès (southern*
980 *Pyrenees. NE Spain). Quaternary Research 78. 323-332.*

981 *Corella. J.P.. Stefanova. V.. El Anjoumi. A.. Rico. E.. Giralt. S.. Moreno. A..*
982 *Plata-Montero. A.. Valero-Garcés. B.L.. 2013. A 2500-year multi-proxy reconstruction*
983 *of climate change and human activities in northern Spain: The Lake Arreo record.*
984 *Palaeogeography. Palaeoclimatology. Palaeoecology 386. 555-568.*

Corella. J.P.. Valero-Garcés. B.L.. Wang. F.. Martínez-Cortizas. A.. Cuevas. C.. Saiz-Lopez. A.. 2017. 700 years reconstruction of mercury and lead atmospheric deposition in the Pyrenees (NE Spain). Atmospheric environment 155. 97-107.

Csavina. J.. Field. J.. Taylor. M.P.. Gao. S.. Landázuri. A.. Betterton. E.A.. Sáez. A.E.. 2012. A review on the importance of metals and metalloids in atmospheric dust and aerosol from mining operations. Science of the Total Environment 433. 58-73.

de Blas, M. A. 1996. La primera minería metálica del N. Peninsular: las indicaciones del C-14 y la cronología prehistórica de las explotaciones del Aramo y el Milagro. Complutum extra, 217-266.

de Blas. M.A.. 2005.Un témoignage probant de l'exploitation préhistorique du cuivre dansle nord de la péninsule ibérique: le complexe minier de l'Aramo. Mém. S. Préhist. F.37. 195–205

Dee. D.P.. Uppala. S.. Simmons. A.. Berrisford. P.. Poli. P.. Kobayashi. S.. Andrae. U.. Balmaseda. M.. Balsamo. G.. Bauer. d.P.. 2011. The ERA-Interim reanalysis: Configuration and performance of the data assimilation system. Quarterly Journal of the royal meteorological society 137. 553-597.

Díez. E.G.. Corella. J.P.. Adatte. T.. Thevenon. F.. Loizeau. J.-L.. 2017. High-resolution reconstruction of the 20th century history of trace metals. major elements. and organic matter in sediments in a contaminated area of Lake Geneva. Switzerland. Applied Geochemistry 78. 1-11.

Draxler. R.R.. Stunder. B.. Rolph. G.. Taylor. J.. 2009. NOAA Air Resources Laboratory. Silver Spring. MD. December 1997. revised January 2009. http://www.arl.noaa. gov/documents/reports/hysplit_user_ guide.pdf.

Elbaz-Poulichet. F.. Dezileau. L.. Freydier. R.. Cossa. D.. Sabatier. P.. 2011. A 3500-year record of Hg and Pb contamination in a Mediterranean sedimentary archive

(The Pierre Blanche Lagoon. France). Environmental Science & Technology 45. 8642-8647.

Elbaz-Poulichet. F.. Guédron. S.. Anne-Lise. D.. Freydier. R.. Perrot. V.. Rossi. M.. Piot. C.. Delpoux. S.. Sabatier. P.. 2020. A 10.000-year record of trace metal and metalloid (Cu. Hg. Sb. Pb) deposition in a western Alpine lake (Lake Robert. France): Deciphering local and regional mining contamination. Quaternary Science Reviews 228. 106076.

EMEP. European Monitoring and Evaluation Programme http://emep.int.

Enrico. M.. Le Roux. G.. Heimbürger. L.-E.. Van Beek. P.. Souhaut. M.. Chmeleff. J.r.. Sonke. J.E.. 2017. Holocene atmospheric mercury levels reconstructed from peat bog mercury stable isotopes. Environmental Science & Technology 51. 5899-5906.

Faïn. X.. Ferrari. C.P.. Dommergue. A.. Albert. M.R.. Battle. M.. Severinghaus. J.. Arnaud. L.. Barnola. J.-M.. Cairns. W.. Barbante. C.. 2009. Polar firn air reveals large-scale impact of anthropogenic mercury emissions during the 1970s. Proceedings of the National Academy of Sciences 106. 16114-16119.

Fanlo. I.. Touray. C.J.. Subías. I.. Fernández-Nieto. C.. 1998. Geochemical patterns of a sheared fluorite vein. Parzan. Spanish Central Pyrenees. Mineralium Deposita 33. 620-632.

Gallego. J.L.. Ortiz. J.E.. Sánchez-Palencia. Y.. Baragaño. D.. Borrego. Á.G.. Torres. T.. 2019. A multivariate examination of the timing and accumulation of potentially toxic elements at Las Conchas bog (NW Spain). Environmental Pollution 254. 113048.

García-Alix. A.. Jiménez-Espejo. F.J.. Lozano. J.A.. Jiménez-Moreno. G.. Martínez-Ruiz. F.. Sanjuán. L.G.. Jiménez. G.A.. Alfonso. E.G.. Ruiz-Puertas. G..

Anderson. R.S.. 2013. Anthropogenic impact and lead pollution throughout the Holocene in Southern Iberia. Science of the Total Environment 449. 451-460.

García-Ruiz. J.M.. López-Moreno. J.I.. Lasanta. T.. Vicente-Serrano. S.M.. González-Sampériz. P.. Valero-Garcés. B.L.. Sanjuán. Y.. Beguería. S.. Nadal-Romero. E.. Lana-Renault. N.. 2015. Geo-ecological effects of Global Change in the Central Spanish Pyrenees: A review at different spatial and temporal scales. Pirineos 170. e012.

García-Ruiz. J.M.. Palacios. D.. de Andrés. N.. Valero-Garcés. B.L.. López-Moreno. J.I.. Sanjuán. Y.. 2014. Holocene and 'little ice age'glacial activity in the Marboré cirque. Monte Perdido Massif. Central Spanish Pyrenees. The Holocene 24. 1439-1452.

George. L.L.. Cook. N.J.. Crowe. B.B.. Ciobanu. C.L.. 2018. Trace elements in hydrothermal chalcopyrite. Mineralogical Magazine 82. 59-88.

Girard. J.. Munoz. M.. Cauuet. B.. Polve. M.. Aries. S.. Callegarin. L.. 2010. Silver Mines on the Massif of Montaigu (Hautes-Pyrénées. France): An Aquitanian Network for Silver? Study on Lead Isotopes. ArchéoSciences. 235-242.

Goldwater. L.J.. 1972. Mercury: a history of quicksilver. Baltimore: York Press

González-Sampériz. P.. Aranbarri. J.. Pérez-Sanz. A.. Gil-Romera. G.. Moreno. A.. Leunda. M.. Sevilla-Callejo. M.. Corella. J.P.. Morellón. M.. Oliva. B.. 2017. Environmental and climate change in the southern Central Pyrenees since the Last Glacial Maximum: A view from the lake records. Catena 149. 668-688.

González-Sampériz. P.. Montes. L.. Aranbarri. J.. Leunda. M.. Domingo. R.. Laborda. R.. Sanjuan. Y.. Gil-Romera. G.. Lasanta. T.. García-Ruiz. J.. 2019. Scenarios. timing and paleo-environmental indicators for the identification of Anthropocene in the vegetal landscape of the Central Pyrenees (NE Iberia). Cuadernos de Investigación Geográfica 45. 167-193.

Guyard. H.. Chapron. E.. St-Onge. G.. Anselmetti. F.S.. Arnaud. F.. Magand. O.. Francus. P.. Mélières. M.-A.. 2007. High-altitude varve records of abrupt environmental changes and mining activity over the last 4000 years in the Western French Alps (Lake Bramant. Grandes Rousses Massif). quaternary science reviews 26. 2644-2660.

Hamilton-Taylor. J.. Davison. W.. 1995. Redox-driven cycling of trace elements in lakes. Physics and chemistry of lakes. Springer. pp. 217-263.

Hanebuth. T.J.. King. M.L.. Mendes. I.. Lebreiro. S.. Lobo. F.J.. Oberle. F.K.. Antón. L.. Ferreira. P.A.. Reguera. M.I.. 2018. Hazard potential of widespread but hidden historic offshore heavy metal (Pb. Zn) contamination (Gulf of Cadiz. Spain). Science of the Total Environment 637. 561-576.

Hansson. S.V.. Claustres. A.. Probst. A.. De Vleeschouwer. F.. Baron. S.. Galop. D.. Mazier. F.. Le Roux. G.. 2017. Atmospheric and terrigenous metal accumulation over 3000 years in a French mountain catchment: Local vs distal influences. Anthropocene 19. 45-54.

Hansson. S.V.. Grusson. Y.. Chimienti. M.. Claustres. A.. Jean. S.. Le Roux. G.. 2019. Legacy Pb pollution in the contemporary environment and its potential bioavailability in three mountain catchments. Science of the Total Environment 671. 1227-1236.

Hernández. A. 2007. Los mineros del azogue. Fundación Almadén 'Francisco Javier de Villegas'. Almaden.

Hillman. A.L.. Abbott. M.B.. Valero-Garcés. B.. Morellon. M.. Barreiro-Lostres. F.. Bain. D.J.. 2017. Lead pollution resulting from Roman gold extraction in northwestern Spain. The Holocene 27. 1465-1474.

Hong. S.. Candelone. J.-P.. Patterson. C.C.. Boutron. C.F.. 1994. Greenland ice evidence of hemispheric lead pollution two millennia ago by Greek and Roman civilizations. Science 265. 1841-1843.

Hong. S.. Candelone. J.-P.. Patterson. C.C.. Boutron. C.F.. 1996. History of ancient copper smelting pollution during Roman and medieval times recorded in Greenland ice. Science 272. 246-249.

Horowitz. H.M.. Jacob. D.J.. Zhang. Y.. Dibble. T.S.. Slemr. F.. Amos. H.M.. Schmidt. J.A.. Corbitt. E.S.. Marais. E.A.. Sunderland. E.M.. 2017. A new mechanism for atmospheric mercury redox chemistry: implications for the global mercury budget. Atmospheric Chemistry and Physics 17. 6353-6371.

Hylander. L.D.. Meili. M.. 2003. 500 years of mercury production: global annual inventory by region until 2000 and associated emissions. Science of the Total Environment 304. 13-27.

Irabien. M.J.. Cearreta. A.. Urteaga. M.. 2012. Historical signature of Roman mining activities in the Bidasoa estuary (Basque Country. northern Spain): an integrated micropalaeontological. geochemical and archaeological approach. Journal of Archaeological Science 39. 2361-2370.

Killick. D.. Fenn. T.. 2012. Archaeometallurgy: the study of preindustrial mining and metallurgy. Annual Review of Anthropology 41.

Komárek. M.. Ettler. V.. Chrastný. V.. Mihaljevič. M.. 2008. Lead isotopes in environmental sciences: a review. Environment International 34. 562-577.

Kylander. M.E.. Weiss. D.J.. Cortizas. A.M.. Spiro. B.. Garcia-Sanchez. R.. Coles. B.. 2005. Refining the pre-industrial atmospheric Pb isotope evolution curve in Europe using an 8000 year old peat core from NW Spain. Earth and Planetary Science Letters 240. 467-485.

Lavilla. I.. Filgueiras. A.. Valverde. F.. Millos. J.. Palanca. A.. Bendicho. C.. 2006. Depth profile of trace elements in a sediment core of a high-altitude lake deposit at the Pyrenees. Spain. Water. air. and soil pollution 172. 273-293.

Le Roux. G.. Fagel. N.. De Vleeschouwer. F.. Krachler. M.. Debaille. V.. Stille. P.. Mattielli. N.. Van Der Knaap. W.O.. Van Leeuwen. J.F.. Shotyk. W.. 2012. Volcano-and climate-driven changes in atmospheric dust sources and fluxes since the Late Glacial in Central Europe. Geology 40. 335-338.

Le Roux. G.. Hansson. S.V.. Claustres. A.. Binet. S.. De Vleeschouwer. F.. Gandois. L.. Mazier. F.. Simonneau. A.. Teisserenc. R.. Allen. D.. 2019. Trace Metal Legacy in Mountain Environments. Biogeochemical Cycles. 191-206.

Leblanc. M.. Morales. J.. Borrego. J.. Elbaz-Poulichet. F.. 2000. 4.500-year-old mining pollution in southwestern Spain: long-term implications for modern mining pollution. Economic Geology 95. 655-662.

Leunda. M.. Gil-Romera. G.. Daniau. A.-L.. Benito. B.M.. González-Sampériz. P.. 2020. Holocene fire and vegetation dynamics in the Central Pyrenees (Spain). Catena 188. 104411.

Leunda. M.. González-Sampériz. P.. Gil-Romera. G.. Aranbarri. J.. Moreno. A.. Oliva-Urcia. B.. Sevilla-Callejo. M.. Valero-Garcés. B.. 2017. The Late-Glacial and Holocene Marboré Lake sequence (2612 m asl. Central Pyrenees. Spain): testing high altitude sites sensitivity to millennial scale vegetation and climate variability. Global and planetary change 157. 214-231.

López-Costas. O.. Kylander. M.. Mattielli. N.. Álvarez-Fernández. N.. Pérez-Rodríguez. M.. Mighall. T.. Bindler. R.. Cortizas. A.M.. 2020. Human bones tell the story of atmospheric mercury and lead exposure at the edge of Roman World. Science of the Total Environment 710. 136319.

MacDonald. D.D.. Ingersoll. C.G.. Berger. T.A.. 2000. Development and evaluation of consensus-based sediment quality guidelines for freshwater ecosystems. Arch. Environ. Contam. Toxicol. 39. 20-31.

Manteca. J.-I.. Ros-Sala. M.. Ramallo-Asensio. S.. Navarro-Hervás. F.. Rodríguez-Estrella. T.. Cerezo-Andreo. F.. Ortiz-Menéndez. J.-E.. de-Torres. T.. Martínez-Andreu. M.. 2017. Early metal pollution in southwestern Europe: the former littoral lagoon of El Almarjal (Cartagena mining district. SE Spain). A sedimentary archive more than 8000 years old. Environmental Science and Pollution Research 24. 10584-10603.

Mariet. A.-L.. Monna. F.. Gimbert. F.. Bégeot. C.. Cloquet. C.. Belle. S.. Millet. L.. Rius. D.. Walter-Simonnet. A.-V.. 2018. Tracking past mining activity using trace metals. lead isotopes and compositional data analysis of a sediment core from Longemer Lake. Vosges Mountains. France. Journal of Paleolimnology 60. 399-412.

Martín-Puertas. C.. Martínez-Ruiz. F.. Jimenez Espejo. F.J.. Nieto-Moreno. V.. Rodrigo. M.. Mata. M.P.. Valero-Garcés. B.L.. 2010. Late Holocene climate variability in the southwestern Mediterranean region: an integrated marine and terrestrial geochemical approach. Climate of the Past 6. 807-816.

Martínez-Cortizas. A.. Pontevedra-Pombal. X.. Munoz. J.N.. García-Rodeja. E.. 1997. Four thousand years of atmospheric Pb. Cd and Zn deposition recorded by the ombrotrophic peat bog of Penido Vello (Northwestern Spain). Water. air. and soil pollution 100. 387-403.

Martínez-Cortizas. A.. Pontevedra-Pombal. X.. García-Rodeja. E.. Nóvoa. M.. J. C.. Shotyk. W.. 1999. Mercury in a Spanish Peat Bog: Archive of Climate Change and Atmospheric Metal Deposition. Science 284. 939-942.

Martínez-Cortizas. A.. Garcia-Rodeja. E.. Pombal X.. P.. Munoz JC.. N.. D.. W.. AK. C.. 2002. Atmospheric Pb deposition in Spain during the last 4600 years recorded by two ombrotrophic peat bogs and implications for the use of peat as archive. Science of the Total Environment 292. 33-44.

Martínez Cortizas. A.. Peiteado Varela. E.. Bindler. R.. Biester. H.. Cheburkin. A.. 2012. Reconstructing historical Pb and Hg pollution in NW Spain using multiple cores from the Chao de Lamoso bog (Xistral Mountains). Geochimica et Cosmochimica Acta 82. 68-78.

Martínez-Cortizas. A.. López-Merino. L.. Bindler. R.. Mighall. T.. Kylander. M.. 2013. Atmospheric Pb pollution in N Iberia during the late Iron Age/Roman times reconstructed using the high-resolution record of La Molina mire (Asturias. Spain). Journal of Paleolimnology 50. 71-86.

Martínez-Cortizas. A.. López-Merino. L.. Bindler. R.. Mighall. T.. Kylander. M.E.. 2016. Early atmospheric metal pollution provides evidence for Chalcolithic/Bronze Age mining and metallurgy in Southwestern Europe. Science of the Total Environment 545. 398-406.

Martínez Cortizas. A.. López-Costas. O.. Orme. L.. Mighall. T.. Kylander. M.E.. Bindler. R.. Gallego Sala. A.. 2020. Holocene atmospheric dust deposition in NW Spain. The Holocene 30. 507-518.

Martinon-Torres. M.. Rehren. T.. 2011. Mining. Europe. Encyclopedia of Society and Culture in the Medieval World. Schlager. Dallas.

McConnell. J.R.. Chellman. N.J.. Wilson. A.I.. Stohl. A.. Arienzo. M.M.. Eckhardt. S.. Fritzsche. D.. Kipfstuhl. S.. Opel. T.. Place. P.F.. Steffensen. J.P.. 2019. Pervasive Arctic lead pollution suggests substantial growth in medieval silver

production modulated by plague. climate. and conflict. Proceedings of the National Academy of Sciences 116. 14910-14915.

McConnell. J.R.. Wilson. A.I.. Stohl. A.. Arienzo. M.M.. Chellman. N.J.. Eckhardt. S.. Thompson. E.M.. Pollard. A.M.. Steffensen. J.P.. 2018. Lead pollution recorded in Greenland ice indicates European emissions tracked plagues. wars. and imperial expansion during antiquity. Proceedings of the National Academy of Sciences 115. 5726-5731.

Mil-Homens. M.. Vale. C.. Brito. P.. Naughton. F.. Drago. T.. Raimundo. J.. Anes. B.. Schmidt. S.. Caetano. M.. 2017. Insights of Pb isotopic signature into the historical evolution and sources of Pb contamination in a sediment core of the southwestern Iberian Atlantic shelf. Science of the Total Environment 586. 473-484.

Montero-Ruiz. I.. Castanyer. P.. Gener. M.. Hunt. M.. Mata. J.. Pons. H.. Rovira-Llorens. S.. Rovira-Hortala. C.. Renzi. M.. Santos-Retolaza. M.. 2007. Lead and silver metallurgy in Emporion (L'Escala. Girona. Spain). Proceedings of the 2nd International Conference on Archeometallurgy in Europe. Aquileia. Italy.

More. A.F.. Spaulding. N.E.. Bohleber. P.. Handley. M.J.. Hoffmann. H.. Korotkikh. E.V.. Kurbatov. A.V.. Loveluck. C.P.. Sneed. S.B.. McCormick. M.. 2017. Next-generation ice core technology reveals true minimum natural levels of lead (Pb) in the atmosphere: Insights from the Black Death. GeoHealth 1. 211-219.

Morellón. M.. Pérez-Sanz. A.. Corella. J.P.. Büntgen. U.. Catalán. J.. González-Sampériz. P.. González-Trueba. J.J.. López-Sáez. J.A.. Moreno. A.. Pla-Rabes. S.. Saz-Sánchez. M.A.. Scussolini. P.. Serrano. E.. Steinhilber. F.. Stefanova. V.. Vegas-Vilarrúbia. T.. Valero-Garcés. B.. 2012. A multi-proxy perspective on millennium-long climate variability in the Southern Pyrenees. Climate of the Past 8. 683-700.

Moreno. A.. Pérez. A.. Frigola. J.. Nieto-Moreno. V.. Rodrigo-Gámiz. M.. Martrat. B.. González-Sampériz. P.. Morellón. M.. Martín-Puertas. C.. Corella. J.P.. Belmonte. Á.. Sancho. C.. Cacho. I.. Herrera. G.. Canals. M.. Grimalt. J.O.. Jiménez-Espejo. F.. Martínez-Ruiz. F.. Vegas-Vilarrúbia. T.. Valero-Garcés. B.L.. 2012. The Medieval Climate Anomaly in the Iberian Peninsula reconstructed from marine and lake records. Quaternary Science Reviews 43. 16-32.

Nicolás-Martínez. P.M.. 2013. Morfología del circo de Tucarroya (Macizo de Monte Perdido. Pirineo aragonés). Cuadernos de Investigación Geográfica 7. 51-80.

Nieto-Callen. J.J.. 1996. El proceso sidero-metalúrgico altoaragones: Los valles de Bielsa y Gistain en la Edad Moderna (1565-1800). Llull 19. 471-507.

Oliva. M.. Ruiz-Fernández. J.. Barriendos. M.. Benito. G.. Cuadrat. J.M.. Domínguez-Castro. F.. García-Ruiz. J.M.. Giralt. S.. Gómez-Ortiz. A.. Hernández. A.. López-Costas. O.. López-Moreno. J.I.. López-Sáez. J.A.. Martínez-Cortizas. A.. Moreno. A.. Prohom. M.. Saz. M.A.. Serrano. E.. Tejedor. E.. Trigo. R.. Valero-Garcés. B.. Vicente-Serrano. S.M.. 2018. The Little Ice Age in Iberian mountains. Earth-Science Reviews 177. 175-208.

Oliva-Urcia. B.. Moreno. A.. Leunda. M.. Valero-Garcés. B.. González-Sampériz. P.. Gil-Romera. G.. Mata. M.. Group. H.. 2018. Last deglaciation and Holocene environmental change at high altitude in the Pyrenees: the geochemical and paleomagnetic record from Marboré Lake (N Spain). Journal of paleolimnology 59. 349-371.

Pèlachs. A.. Nadal. J.. Soriano. J.M.. Molina. D.. Cunill. R.. 2009. Changes in Pyrenean woodlands as a result of the intensity of human exploitation: 2.000 years of metallurgy in Vallferrera. northeast Iberian Peninsula. Vegetation History and archaeobotany 18. 403-416.

Pérez. I.S.. González. I.F.. González. E.M.. SORIA. C.B.. 2008. Explotaciones mineras del entorno del Hospital de Benasque: geología y encuadre histórico. Macla: revista de la Sociedad Española de Mineralogía. 239.

Pey. J.. Querol. X.. Alastuey. A.. Forastiere. F.. Stafoggia. M.. 2013. African dust outbreaks over the Mediterranean Basin during 2001-2011: PM10 concentrations. phenomenology and trends. and its relation with synoptic and mesoscale meteorology. Atmospheric Chemistry and Physics 13. 1395.

Pontevedra-Pombal. X.. Mighall. T.M.. Nóvoa-Muñoz. J.C.. Peiteado-Varela. E.. Rodríguez-Racedo. J.. García-Rodeja. E.. Martínez-Cortizas. A.. 2013. Five thousand years of atmospheric Ni. Zn. As. and Cd deposition recorded in bogs from NW Iberia: prehistoric and historic anthropogenic contributions. Journal of Archaeological Science 40. 764-777.

Preunkert. S.. McConnell. J.R.. Hoffmann. H.. Legrand. M.. Wilson. A.I.. Eckhardt. S.. Stohl. A.. Chellman. N.J.. Arienzo. M.M.. Friedrich. R.. 2019. Lead and antimony in basal ice from Col du Dome (French Alps) dated with radiocarbon: A record of pollution during antiquity. Geophysical Research Letters 46. 4953-4961.

Pujalte. V.. Robador. A.. Payros. A.. Samsó. J.M.. 2016. A siliciclastic braid delta within a lower Paleogene carbonate platform (Ordesa-Monte Perdido National Park. southern Pyrenees. Spain): record of the Paleocene–Eocene thermal maximum perturbation. Palaeogeography. palaeoclimatology. palaeoecology 459. 453-470.

Renberg. I.. Persson. M.W.. Emteryd. O.. 1994. Pre-industrial atmospheric lead contamination detected in Swedish lake sediments. Nature 368. 323-326.

Rodríguez. S.. Cuevas. E.. Prospero. J.. Alastuey. A.. Querol. X.. López-Solano. J.. García. M.. Alonso-Pérez. S.. 2015. Modulation of Saharan dust export by the North African dipole. Atmospheric Chemistry and Physics 15. 7471.

Pérez-Rodríguez. M.. Biester. H.. Aboal. J. R.. Toro. M.. Cortizas. A. M.. 2019. Thawing of snow and ice caused extraordinary high and fast mercury fluxes to lake sediments in Antarctica. Geochimica et Cosmochimica Acta. 248. 109-122.

Rosman. K.J.. Chisholm. W.. Hong. S.. Candelone. J.-P.. Boutron. C.F.. 1997. Lead from Carthaginian and Roman Spanish mines isotopically identified in Greenland ice dated from 600 BC to 300 AD. Environmental Science & Technology 31. 3413-3416.

Rytuba. J.J.. 2003. Mercury from mineral deposits and potential environmental impact. Environmental Geology 43. 326-338.

Salvador. P.. Alonso-Pérez. S.. Pey. J.. Artíñano. B.. Bustos. J.J.d.. Alastuey. A.. Querol. X.. 2014. African dust outbreaks over the western Mediterranean Basin: 11-year characterization of atmospheric circulation patterns and dust source areas. Atmospheric Chemistry & Physics. 14. 6759–6775

Samsó Escolá. J.M.. Robador. A.. 2018. Mapa geológico del Parque Nacional de Ordesa y Monte Perdido. Escala 1:25.000. In: IGME (Ed.). Serie GeoNatur.

Sánchez-España. J.. Mata. M.P.. Vegas. J.. Morellón. M.. Rodríguez. J.A.. Salazar. Á.. Yusta. I.. 2018. Limnochemistry of the remote. high mountain Lake Marboré (Ordesa and Monte Perdido National Park. Central Pyrenees): Stratification dynamics and trace metal anomalies. Limnetica 37. 85-103.

Sánchez-López. G.. Hernández. A.. Pla-Rabes. S.. Toro. M.. Granados. I.. Sigrò. J.. Trigo. R.M.. Rubio-Inglés. M.. Camarero. L.. Valero-Garcés. B.. 2015. The effects of the NAO on the ice phenology of Spanish alpine lakes. Climatic Change 130. 101-113.

Sánchez-López. G.. Hernández. A.. Pla-Rabès. S.. Trigo. R.M.. Toro. M.. Granados. I.. Sáez. A.. Masqué. P.. Pueyo. J.J.. Rubio-Inglés. M.. 2016. Climate reconstruction for the last two millennia in central Iberia: The role of East Atlantic

(EA). North Atlantic Oscillation (NAO) and their interplay over the Iberian Peninsula. Quaternary Science Reviews 149. 135-150.

Serrano. O.. Mateo. M. A.. Dueñas-Bohórquez. A.. Renom. P.. López-Sáez. J. A.. Cortizas. A. M.. 2011. The Posidonia oceanica marine sedimentary record: A Holocene archive of heavy metal pollution. Science of the Total Environment. 409(22). 4831-4840.

Serrano. O.. Martínez-Cortizas. A.. Mateo. M.. Biester. H.. Bindler. R.. 2013. Millennial scale impact on the marine biogeochemical cycle of mercury from early mining on the Iberian Peninsula. Global Biogeochemical Cycles 27. 21-30.

Stein, A.F., Draxler, R.R., Rolph, G.D., Stunde, B.J.B., M. D. Cohen. M.D., Ngan F. 2015. NOAA's HYSPLIT Atmospheric Transport and Dispersion Modeling System. Bull. Amer. Meteor. Soc. 96 (12): 2059–2077.

Stos-Gale. Z.A.. Gale. N.H.. 2009. Metal provenancing using isotopes and the Oxford archaeological lead isotope database (OXALID). Archaeological and Anthropological Sciences 1. 195-213.

Subías. I.. Fanlo. I.. Billström. K.. 2015. Ore-forming timing of polymetallic-fluorite low temperature veins from Central Pyrenees: A Pb. Nd and Sr isotope perspective. Ore Geology Reviews 70. 241-251.

Thalacker. J.G.. 1804. Noticias y descripción de las grandes explotaciones de unas antiguas minas situadas al pie de los Pirineos y en la provincia de Guipúzcoa. Variedades de Ciencias. Literatura y Artes 4. 201-215.

Thevenon. F.. Guédron. S.. Chiaradia. M.. Loizeau. J.-L.. Poté. J.. 2011. (Pre-) historic changes in natural and anthropogenic heavy metals deposition inferred from two contrasting Swiss Alpine lakes. Quaternary Science Reviews 30. 224-233.

1302 *Tylmann. W.. 2005. Lithological and geochemical record of anthropogenic*
1303 *changes in recent sediments of a small and shallow lake (Lake Pusty Staw. northern*
1304 *Poland). Journal of Paleolimnology 33. 313-325.*
1305 *Urteaga. M.. 2014. Minería romana en el Cantábrico Oriental. Cuadernos de*
1306 *Prehistoria y Arqueología de la Universidad de Granada 24. 267-300.*
1307 *Valero-Garcés. B.L.. Oliva-Urcia. B.. Moreno Caballud. A.. Rico. M.T.. Mata-*
1308 *Campo. M.P.. Salazar-Rincón. A.. Rieradevall. M.. García-Ruiz. J.M.. Chueca Cía. J..*
1309 *González-Sampériz. P.. 2013. Dinámica glacial. clima y vegetación en el Parque*
1310 *Nacional de Ordesa y Monte Perdido durante el Holoceno. Proyectos de Investigación*
1311 *en Parques Nacionales: 2009-2012 (MAGRAMA). 7-37*
1312 *Velasco. F.. Pesquera. A.. Herrero. J.. 1996. Lead isotope study of Zn-Pb ore*
1313 *deposits associated with the Basque-Cantabrian basin and Paleozoic basement.*
1314 *northern Spain. Mineralium Deposita 31. 84-92.*
1315 *Vidal. R.. 2012. La minería metálica prehistórica en la Península Ibérica.*
1316 *Lurralde: invest. espac. 35. 67-78.*
1317 *Weiss. D.. Shotyk. W.. Appleby. P.G.. Kramers. J.D.. Cheburkin. A.K.. 1999.*
1318 *Atmospheric Pb deposition since the industrial revolution recorded by five Swiss peat*
1319 *profiles: enrichment factors. fluxes. isotopic composition. and sources. Environmental*
1320 *Science & Technology 33. 1340-1352.*
1321 *Wilhelm. B.. Vogel. H.. Anselmetti. F.. 2017. A multi-centennial record of past*
1322 *floods and earthquakes in Valle d'Aosta. Mediterranean Italian Alps. Natural Hazards*
1323 *and Earth System Sciences 17. 613-625.*
1324 *Wilson. A.. 2002. Machines. power and the ancient economy. The Journal of*
1325 *Roman Studies 92. 1-32.*

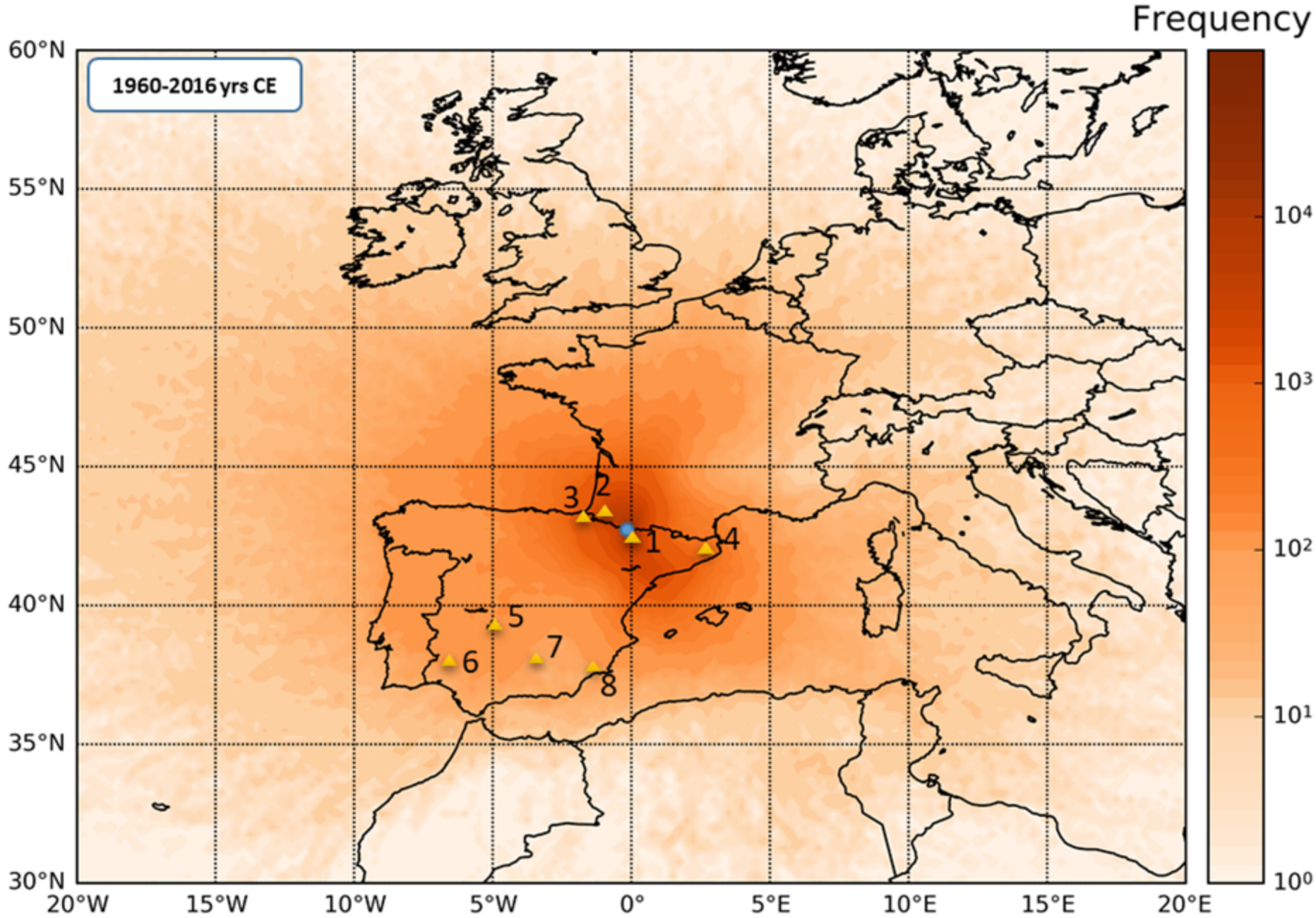
Frequency
1960-2016 yrs CE
60°N
55°N
50°N
45°N
40°N
35°N
30°N
20°W
15°W
10°W
5°W
0°
5°E
10°E
15°E
20°E
10^4
10^3
10^2
10^1
10^0
1
2
3
4
5
6
7
8

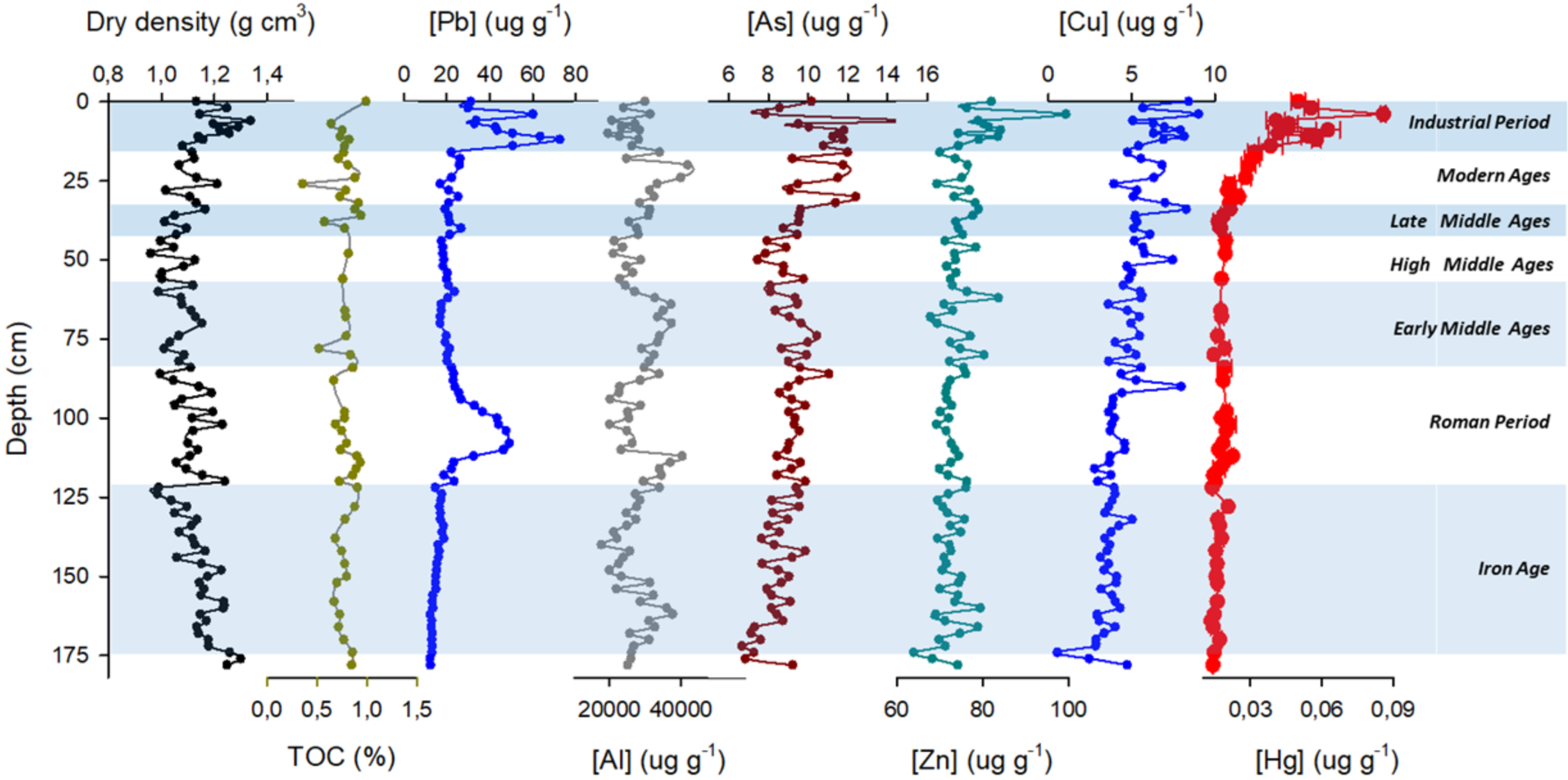
Dry density (g cm3)
[Pb] (ug g-1)
[As] (ug g-1)
[Cu] (ug g-1)
0,8 1,0 1,2 1,4
0 20 40 60 80
6 8 10 12 14 16
0 5 10
Depth (cm)
0 25 50 75 100 125 150 175
Industrial Period
Modern Ages
Late Middle Ages
High Middle Ages
Early Middle Ages
Roman Period
Iron Age
0,0 0,5 1,0 1,5
TOC (%)
20000 40000
[Al] (ug g-1)
60 80 100
[Zn] (ug g-1)
0,03 0,06 0,09
[Hg] (ug g-1)

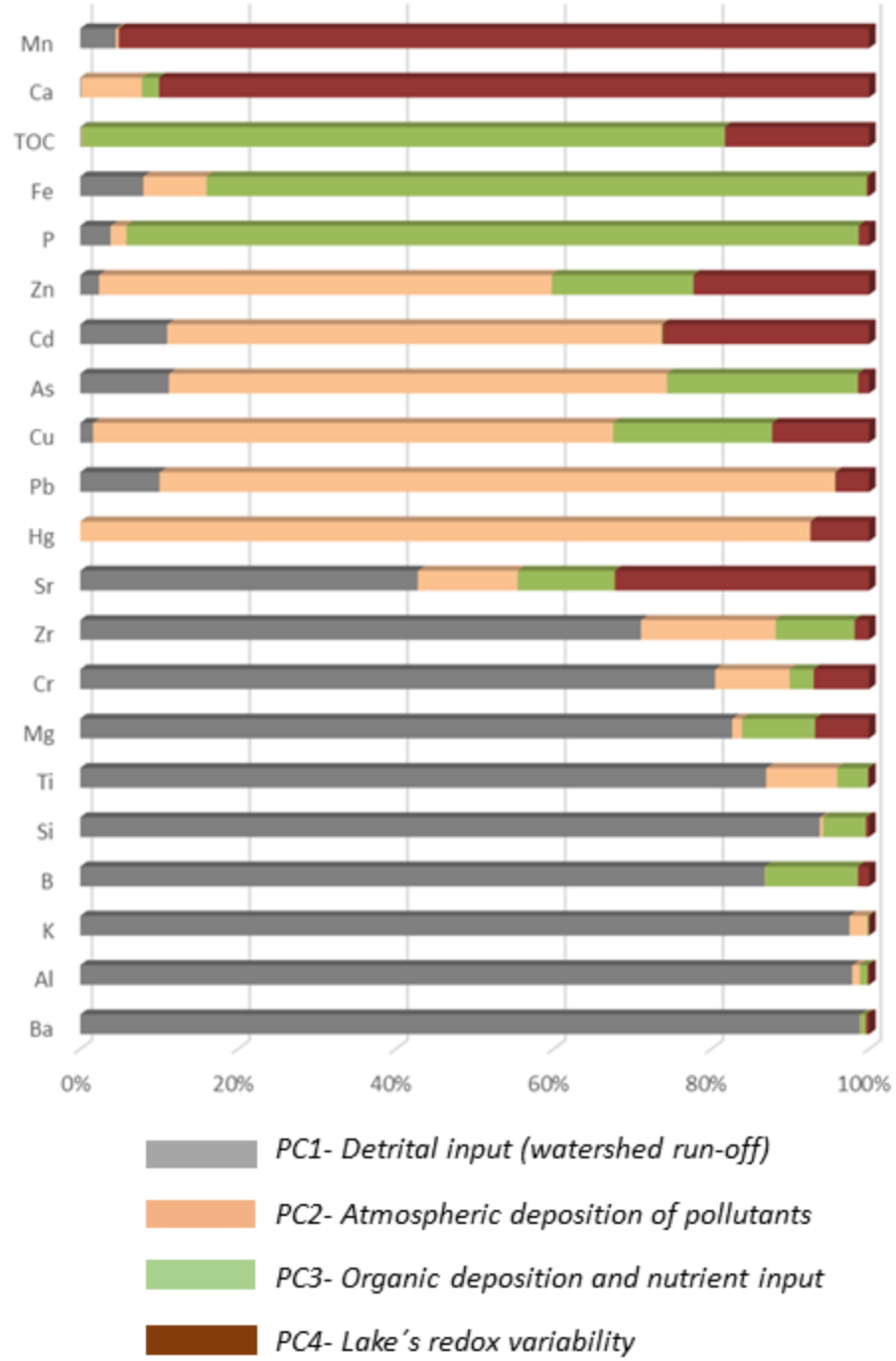
Mn
Ca
TOC
Fe
P
Zn
Cd
As
Cu
Pb
Hg
Sr
Zr
Cr
Mg
Ti
Si
B
K
Al
Ba
0%
20%
40%
60%
80%
100%
PC1- Detrital input (watershed run-off)
PC2- Atmospheric deposition of pollutants
PC3- Organic deposition and nutrient input
PC4- Lake´s redox variability

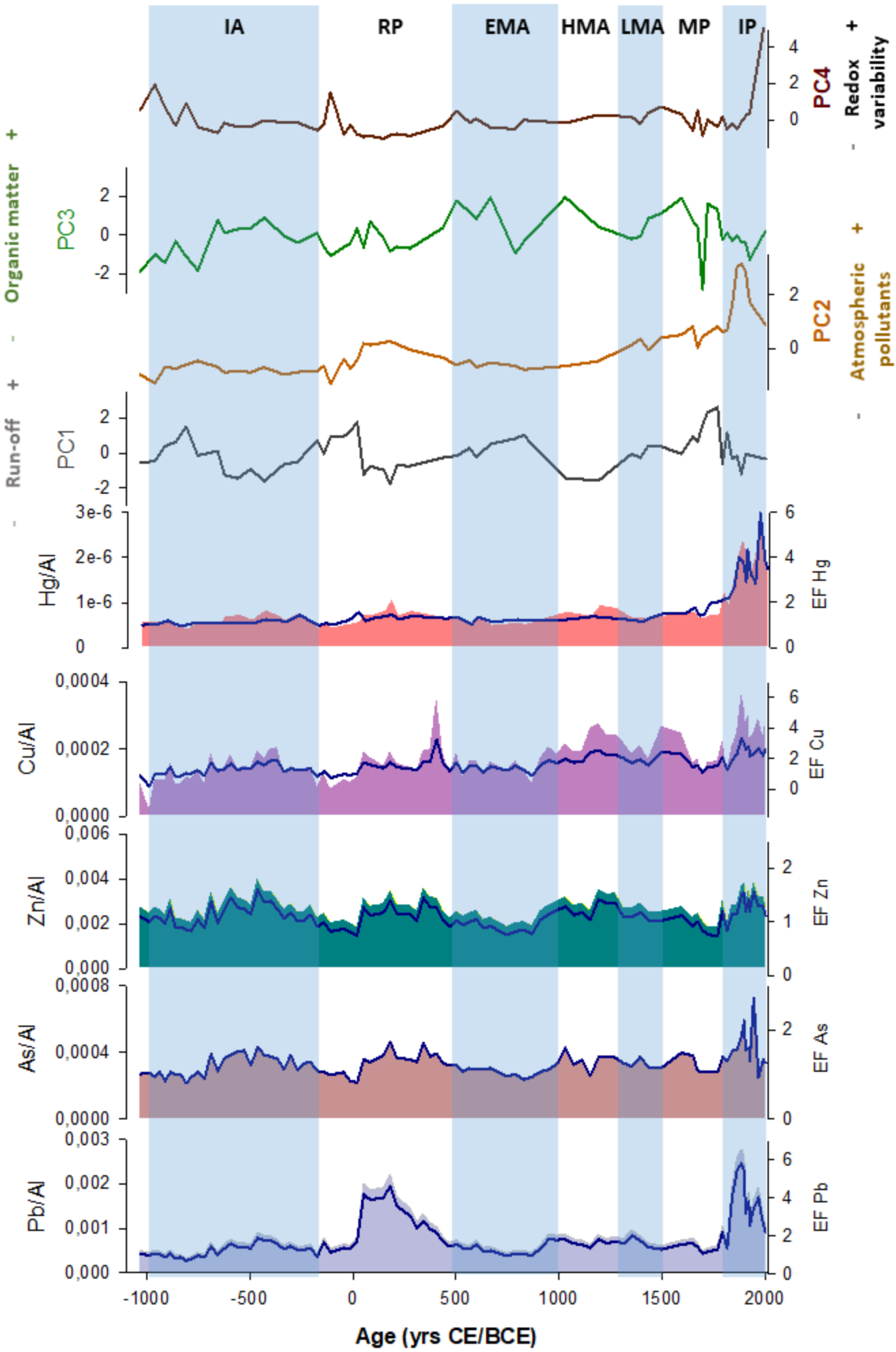
IA
RP
EMA
HMA
LMA
MP
IP
PC4
Redox variability
+
-
PC3
Organic matter
PC2
Atmospheric pollutants
PC1
Run-off
Hg/Al
EF Hg
Cu/Al
EF Cu
Zn/Al
EF Zn
As/Al
EF As
Pb/Al
EF Pb
Age (yrs CE/BCE)

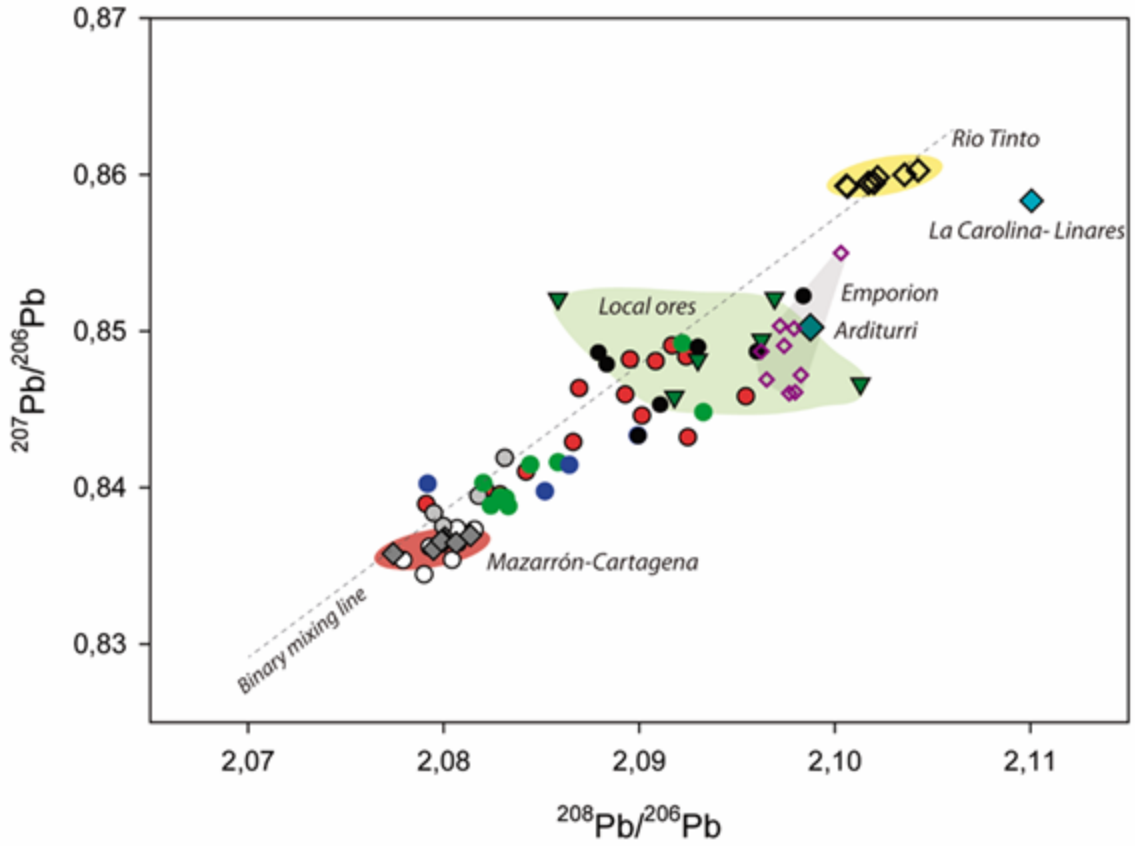

Ore deposits from spanish mines

- La Carolina - Linares
- Rio Tinto
- Mazarrón - Cartagena
- Arditurri
- Local ore deposits and small-scale mines in Central Pyrenees
- Emporion

Lake Marbore

- Late Iron/Iberian Period
- Roman Period
- Migration Period
- Middle Ages
- Modern Period
- Industrial Period

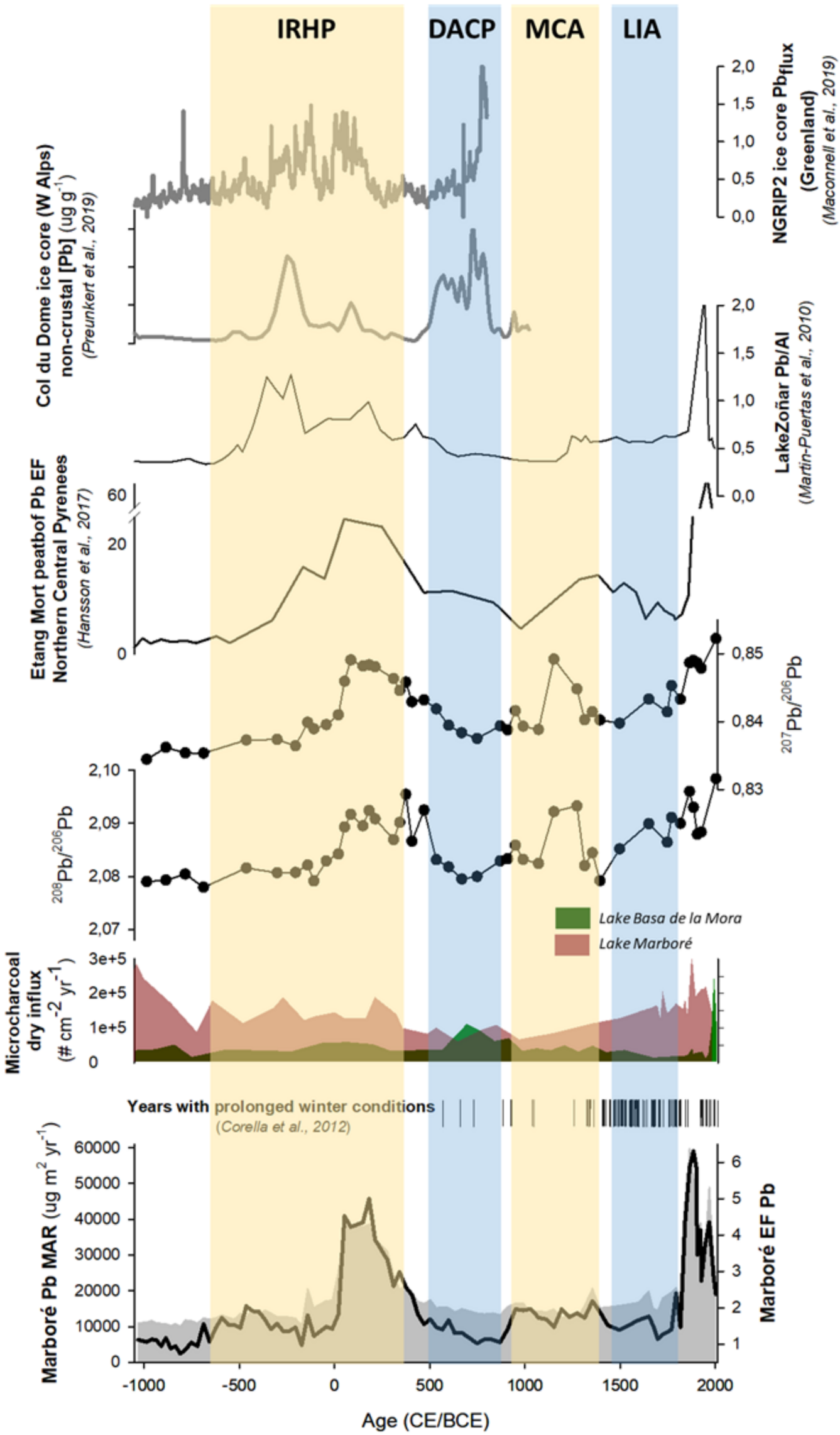
IRHP
DACP
MCA
LIA
Col du Dome ice core (W Alps) non-crustal [Pb] (ug g-1) (Preunkert et al., 2019)
NGRIP2 ice core Pbflux (Greenland) (Maconnell et al., 2019)
2,0
1,5
1,0
0,5
0,0
LakeZoñar Pb/Al (Martin-Puertas et al., 2010)
Etang Mort peatbof Pb EF Northern Central Pyrenees (Hansson et al., 2017)
60
20
0
207Pb/206Pb
0,85
0,84
0,83
208Pb/206Pb
2,10
2,09
2,08
2,07
Lake Basa de la Mora
Lake Marboré
Microcharcoal dry influx (# cm-2 yr-1)
3e+5
2e+5
1e+5
0
Years with prolonged winter conditions
(Corella et al., 2012)
Marboré Pb MAR (ug m2 yr-1)
60000
50000
40000
30000
20000
10000
0
Marboré EF Pb
6
5
4
3
2
1
-1000
-500
0
500
1000
1500
2000
Age (CE/BCE)

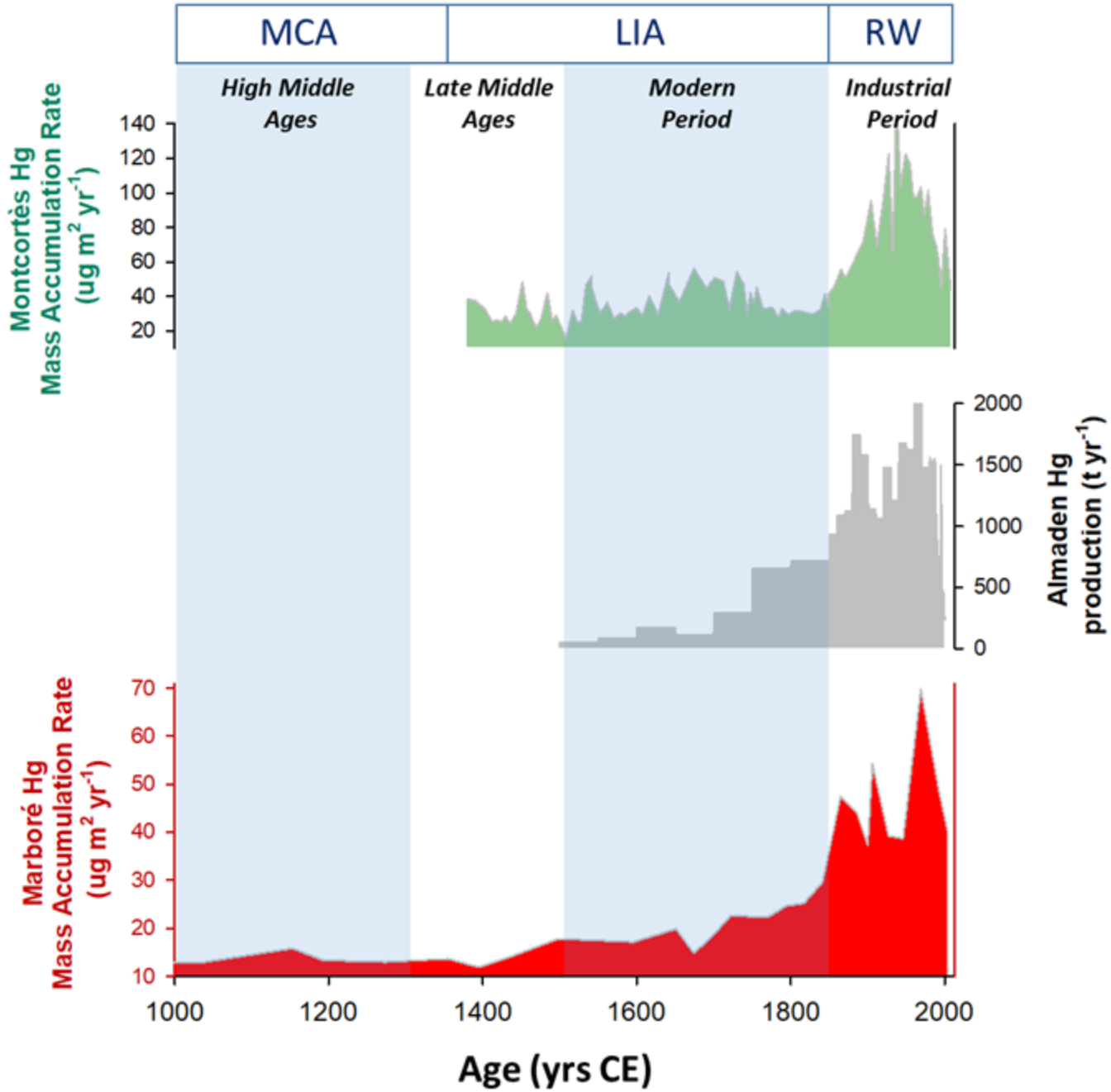
MCA
LIA
RW
High Middle Ages
Late Middle Ages
Modern Period
Industrial Period
Montcortès Hg Mass Accumulation Rate (ug m2 yr-1)
140
120
100
80
60
40
20
2000
1500
1000
500
0
Almaden Hg production (t yr-1)
Marboré Hg Mass Accumulation Rate (ug m2 yr-1)
70
60
50
40
30
20
10
1000
1200
1400
1600
1800
2000
Age (yrs CE)

Table 1: Back trajectories percentages passing over different regions and arriving Lake Marboré area.

Region	**Longitude**	**Latitude**	**Percentage of back-trajectories /%**
SW France	42.83N - 45.83N	1.83W - 0.83E	51.9
Ebro valley	40.00N - 42.50E	1.83W - 2.83E	52.1
Central and western Spain	40.00N - 42.00N	10.00W - 2.5W	16.4
Southern Spain	36.00N - 40.00N	10.00W - 1.00E	17.4
Northern Africa	30.00N - 36.00N	10.00W - 5.00E	3.0

Table 2: Results of the Principal Component Analyses using the scores (loading factors) of the extracted principal components obtained for the geochemical datasets.

Element	**PC1**	**PC2**	**PC3**	**PC4**
Ba	0.98	-0.03	0.08	0.06
Al	0.97	-0.10	0.10	0.04
K	0.95	-0.14	0.04	0.01
B	0.91	0.03	0.33	0.12
Si	0.89	-0.06	-0.22	0.06
Ti	0.88	0.28	0.19	0.03
Mg	0.85	0.10	0.29	0.25
Cr	0.85	0.29	0.16	0.25
Zr	0.81	0.39	0.30	0.13
Sr	0.63	0.34	0.34	0.54
Hg	-0.01	0.90	-0.02	0.26
Pb	-0.26	0.77	-0.02	-0.17
Cu	0.12	0.73	0.41	0.32
As	0.30	0.71	0.44	-0.10
Cd	0.27	0.64	-0.03	0.41
Zn	0.12	0.59	0.33	0.37
P	0.18	0.13	0.88	-0.10
Fe	0.26	0.26	0.83	0.05
TOC	0.03	-0.02	0.72	0.34
Ca	0.03	0.25	0.13	0.85
Mn	0.15	0.04	0.00	0.68
PCA variance	*46.70*	*19.57*	*8.69*	*6.88*
Accumulated variance	*46.70*	*66.27*	*74.96*	*81.84*

Reconstruction of the mining-related pollution legacy in high-altitude lacustrine ecosystems